Chapter 5
Plasma Heating and Current Drive

Thomas J. Dolan

Objectives

After reading this chapter one should understand

Ohmic heating
Heating by beam injection and by alpha particles
Heating by waves using various plasma resonances
Equipment used in heating systems for large experiments.

5.1 Introduction

An electric stove utilizes the I^2R ohmic heating power generated by flow of an electric current I through a heating element with resistance R. A diesel engine heats its fuel-air mixture to ignition temperature by compression. A microwave oven heats food by absorption of electromagnetic waves. Electron beam welders heat the metal to be welded by the impact of energetic electron beams. The principle methods of plasma heating are these four plus alpha particle heating:

- Ohmic heating—current flow through plasma.
- Compression—by magnetic field, shock wave, or beam pressure.
- Wave heating—radio waves, microwaves, laser beams.
- Particle beam injection—electron beams, ion beams, or neutral beams.
- Heating by 3.5 MeV alpha particles slowing down in the plasma.

For example, to heat a fusion plasma to ignition conditions, if $n = 10^{20}$ m^{-3}, $T = 10$ keV, $V = 200$ m^3, then the plasma thermal energy $W = 1.5n(T_e + T_i) V \approx 100$ MJ. (Note that the temperatures must be converted from keV to J in this equation). If the energy confinement time were 2 s, then the plasma would

T. J. Dolan (✉)
NPRE Department, University of Illinois, Urbana, IL 61801, USA
e-mail: dolantj@illinois.edu

Fig. 5.1 The general heating methods used in ITER. Although the neutral beam is injected against the plasma current in this drawing (counter-injection), injection parallel to the current (co-injection) is used more often. The NBI momentum influences plasma toroidal rotation. Used by permission of United Kingdom Atomic Energy Authority
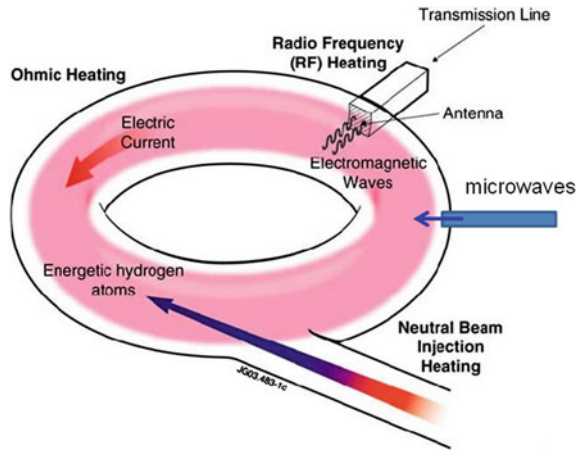
lose about 50 MJ/s of energy, so a heating power >50 MW would be needed to raise the temperature to ignition temperatures. This heating power estimate could be reduced on account of fusion product alpha particles heating the plasma, but increased somewhat by radiation losses, which are not accounted for in the usual definition of energy confinement time.

Tokamaks require non-inductive current drive for steady-state operation, and the required current drive power limits the attainable energy gain ratio Q. Current drive methods also heat the plasma, but not all heating methods generate substantial plasma current density.

The ITER experiment will use three external heating methods: ohmic heating, neutral beam injection (NBI), and electromagnetic waves, Fig. 5.1.

A plasma heating method for a reactor should have the following characteristics:

- High power flux, so small ports may be used in the chamber walls.
- High efficiency of generation and transmission.
- Large fraction of energy absorbed in plasma.
- Steady state operation (or *very long* pulses).
- Reliable operation.
- Long-lived, low-activation materials in the waveguides and launchers.
- Control of gas flow between heating source and plasma chamber (such as a cryopump in a neutral beam injection system or a waveguide window).
- Low neutron streaming through the blanket.
- Easy maintenance.
- Low capital cost per Watt of injected power.

5.2 Alpha Particle Heating

Alpha particles produced by fusion reactions will heat plasma electrons and ions collisionally as they slow down. Some alphas may have bad orbits and leave the plasma quickly, but, if the magnetic field configuration is good, most of them will

stay in the plasma until they have lost most of their energy. For example, some 3D computer codes for magnetic field design in stellarators compute the orbits of many alphas to optimize their retention.

Let n_*, m_*, q_*, and T_* be the density, mass, charge, and temperature of the Maxwellian "field particles" (plasma ions and electrons). The alpha energy loss rate dW/dt to electrons and ions can be computed from Coulomb collision theory. The result may be written

$$dW/dt = -\Sigma n_* q^2 q_*^2 b_* L \ H(x, m_*/m)/(4\pi\varepsilon_0^2 m_*) \qquad (5.1)$$

where the summation is over field particle species, $L \sim 18$ is the Coulomb logarithm, ε_o is the permittivity of free space, m = alpha mass, $x = (m_* W/mT_*)^{1/2}$, $b_* = (m*/2kT*)^{1/2}$, and

$$H(x, m_*/m) = erf(x)/x - (2/\pi^{1/2})(1 + m_*/m)exp(-x^2) \qquad (5.2)$$

and erf(x) is the error function (Appendix C) (Dolan 1982). If $x > 2$, then $H = 1/x$, except for impurities heavier than alpha particles. Figure 5.2 shows H as a function of x and m_*/m.

At first most of the alpha energy loss is to electrons, but when their energy W is $<15 \ T_e$ the loss rate to plasma ions becomes dominant (Goldston and Rutherford 1995). The fraction of total alpha energy that goes to electrons and ions are shown in Fig. 5.3, assuming losses to impurities are negligible.

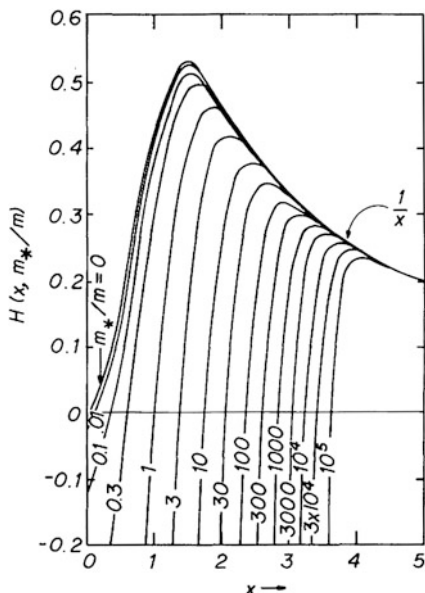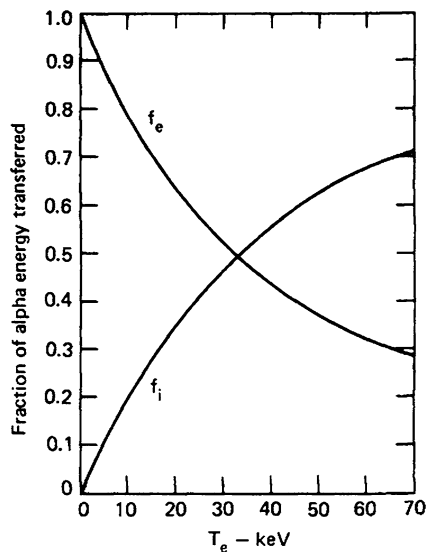**Fig. 5.2** The H function versus x, for various mass ratios (Dolan 1982)

Fig. 5.3 Fraction of alpha
particle energy that go to
electrons and ions during
slowing down to thermal
energies, as functions of
electron temperature (Dolan
1982)

The time that it takes for an alpha particle to slow down in a plasma is approximately

$$\tau_\alpha = C/n_{20}$$

where n_{20} = plasma density in units of 10^{20} m^{-3}, C = 0.45 s at T_e = 10 keV, and C = 0.9 s at T_e = 20 keV (Sheffield 1994).

Fast alpha particles also contribute significantly to the plasma pressure and beta value, which can lead to instability if beta becomes too high. If the alpha density becomes more than a few percent, the fusion power drops significantly, due to dilution of the DT fuel, so very long alpha confinement can be deleterious. For example, in one estimate a 10 % alpha density fraction reduced the fusion power density by a factor of about 2 (Sheffield 1994).

If f_α is the fraction of alpha particle energy retained in the plasma, then the alpha heating power in a DT plasma with fuel ion density n is

$$P_\alpha = (1/4)f_\alpha n^2 \langle \sigma v \rangle_{DT} W_\alpha \tag{5.3}$$

where $\langle \sigma v \rangle_{DT}$ is the reaction rate parameter (Chap. 1) and $W_\alpha = 3.5$ MeV = 5.61×10^{-13} J.

For example, if $f_\alpha = 0.9$, n = 10^{20} m^{-3} and T = 15 keV, then $\langle \sigma v \rangle_{DT} = 2.65 \times 10^{-22}$ m^3/s, and $P_\alpha = 0.33$ MW/m^3. For this case approximately 70 % of the alpha heating goes to electrons and 30 % to ions (Fig. 5.3).

The fusion power density varies with radial position and the alpha particles diffuse radically as they slow down, so this equation gives only an average for the whole plasma.

The Fokker–Planck equation provides a more accurate description of energetic ions slowing down in a plasma (Goldston and Rutherford 1995).

5.3 Ohmic Heating

Plasma currents and $\mathbf{E} \times \mathbf{B}$ drifts may be driven by magnetic induction or by metallic electrodes in contact with the plasma. The power dissipated per unit volume is

$$P = E_{\parallel}J_{\parallel} + E_{\perp}J_{\perp} = \eta_{\parallel}J_{\parallel}^2 + \eta_{\perp}J_{\perp}^2 \; \left(W/m^3\right) \tag{5.4}$$

where the components are parallel or perpendicular to the magnetic field. By definition

$$\eta_{\parallel} = E_{\parallel}/J_{\parallel} = E_z/neu_{ez}, \tag{5.5}$$

Taking the z direction parallel to B and equating the accelerating force of the electric field to the frictional force of electron–ion collisions, we find

$$- eE_z = -m_e u_{ez} v_{ei} \rightarrow u_{ez} = eE_z/m_e v_{ei} \tag{5.6}$$

Then

$$\eta_{\parallel} = m_e v_{ei}/ne^2 = 2.38 \times 10^{-9} Z_{eff} L \; T_{ek}^{-3/2} \; (\Omega m) \tag{5.7}$$

An alternative value of the numerical coefficient is 1.65×10^{-9} (Wesson 2011). where L is the "Coulomb logarithm", Z_{eff} is an effective atomic number of the plasma ions, and T_{ek} is the electron temperature in keV. If $Z \approx 1$ and $L \sim 18$, then

$$\eta_{\parallel} \approx 4 \times 10^{-8} T_{ek}^{-3/2} \; (\Omega m) \tag{5.8}$$

For comparison, the resistivity of copper at room temperature is about $2 \times 10^{-8} \; \Omega m$. At temperatures of a few keV, a hydrogen plasma becomes a better conductor than copper. Ohmic heating becomes less effective at high temperatures.

5.3.1 Increased Resistivity

The resistivities given in Eq. (5.8) represent minimum values due to Coulomb collisions, if neutral atoms are present, the resistivity is increased by the ratio $(v_{en} + v_{ei})/v_{ei}$, where v_{en} and v_{ei} are the electron-neutral and electron–ion momentum-transfer collision frequencies. Impurity ions increase the effective value of Z, thus enhancing the resistivity. Effects of toroidal geometry and trapped particles result in "neoclassical" values of $\eta_{\parallel}$. Plasma turbulence can greatly increase the effective resistivity. Turbulence refers to a condition in which many random collective oscillations are excited by microinstabilities. The collective oscillations may be Langmuir plasma oscillations, ion acoustic waves, Alfven waves, etc. Turbulence may increase the resistivity to a value

$$\eta_{\parallel} = m_e v_{eff}/ne^2 \tag{5.9}$$

where n, m_e, e, and v_{eff} are the density, mass, charge, and effective collision frequency of the electrons, and v_{eff} can be much larger than the collisional v_{ei}.

Although plasma turbulence increases resistivity and makes ohmic heating more effective, turbulence also increases plasma energy loss rates, and the high electric fields needed to drive plasma turbulence can lead to electron runaway.

5.3.2 Electron Runaway

The retarding force of electron–ion Coulomb collisions decreases at high relative velocities u. For electrons with high velocities, this frictional force may be less than the force of the applied electric field, and they will be accelerated to even higher velocities, until they are lost or some other energy loss mechanism balances the applied electric field force. Such *runaway electrons* may carry a substantial fraction of the plasma current. The energy they absorb from the electric field does not heat the plasma directly, and they may be poorly confined, resulting in high-energy x-rays when they hit the wall. Thus, the plasma control system of a large tokamak will try to avoid creating runaways.

Ignition could in principle be attained solely by ohmic heating at very high magnetic fields (Wagner 1981), but it would be difficult, so auxiliary heating methods are usually employed.

5.4 Compression

If plasma is compressed slowly, energy losses during compression will prevent effective heating, and the compression is said to be *nonadiabatic*. If plasma is compressed on a time scale much less than the energy confinement time, then the compression can be *adiabatic*, meaning that energy flow across the boundary is negligible. Adiabatic heating is reversible: if the plasma were allowed to expand, it would return to its original temperature. Typical time scales for adiabatic compression are $\tau \sim 0.1$–1 ms. If compression occurs on a much shorter time scale $\tau \sim 1$ μs, then shock waves may form and produce intense irreversible heating.

5.4.1 Shock Heating

In an ordinary gas, a perturbation in density may propagate as a sound wave. The perturbation may be caused by rupturing a diaphragm between gases at different pressures, by detonation of an explosive, or by motion of a "piston", such as an airplane wing, through the gas. The speed of sound is larger at higher densities, as shown in Fig. 5.4a, which makes the velocity at point A larger than that at point B (Fig. 5.4c).

The result is that the higher-density gas portion of the wave at point A catches up with points B and C, producing a very steep wave front, called a shock front
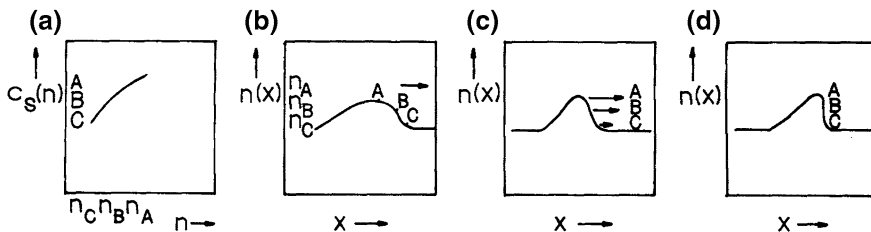
Fig. 5.4 Development of a shock wave. **a** Variation of the sound speed with density. **b** A density perturbation moving to the *right*. **c** Because the density at point *A* is higher, so is its velocity, and it tends to overtake points *B* and *C* resulting in a steep wave front (**d**)

(Fig. 5.4d). The discontinuity of density propagates through the gas, raising the density from n_c to n_A very rapidly, and heating the gas irreversibly. Further "overturning" of the wave is limited by heat conduction and viscosity, so that the shock front develops a certain thickness on the order of a few collisional mean free paths. Such a hydrodynamic shock wave, which propagates via molecular collisions, is probably not of interest for heating fusion reactor plasmas.

Shock waves in plasmas are also caused by the increase of wave speed with density. The wave may be a large-amplitude MHD wave, instead of an ordinary sound wave; and wave propagation is facilitated by changing electromagnetic fields, leaving the plasma in its wake irreversibly heated. In some cases a large current density flows in the wave front. This current-carrying "sheath" acts as a magnetic piston, driving the plasma ahead of it like snow in front of a snowplow. The current may be driven by electrodes in contact with the plasma, or by the electric field induced by pulsed magnet coils. At high temperatures the mean free path for collisions may be very large compared to the shock front thickness, which may be on the order of ρ_i (the ion Larmor radius). Such collisionless shock waves can result in ion temperatures $T_i \sim 10$ keV.

Shock heating is used in some plasma pinch devices (Dolan 1982, Chap. 12). In order to work on microsecond time scales, shock heating coils must have low inductance and operate at high voltage, which leads to a number of technological problems. Since large coils have high inductances, shock heating coils must be small and placed near the plasma, where they will be bombarded by an intense flux of fast neutrons, making them highly radioactive and difficult to replace. The fatigue problems associated with cyclic stresses limit the coil stress and magnetic field to values lower than those attainable in steady-state coils. For these reasons it is unlikely that fusion reactors will use repetitive shock wave heating to ignition.

5.4.2 Adiabatic Compression

The adiabatic equation of state is

$$p_i/n_i^{\gamma} = \text{constant} \tag{5.10}$$

where $p_i = n_i \ T_i = (2/3)n_i\langle W_i\rangle$, n_i = ion density, and $\langle W_i\rangle$ = average ion energy. Using $n_i = N_i/V$, where N_i = total number of ions (assumed constant) in plasma volume V, we can rearrange (5.10) to read

$$\langle W_i\rangle V^{\gamma-1} = \text{constant}$$
$$\gamma = (N + 2)/N \tag{5.11}$$

where N is the number of degrees of freedom during compression. For example, in a one-dimensional compression $\gamma = 3$. Halving the volume would quadruple the ion energy in the direction of compression. A similar relation applies to electrons. Often the average energies will be different in the parallel and perpendicular directions relative to the magnetic field. Then

$$\langle W\rangle = \langle W_\parallel\rangle + \langle W_\perp\rangle$$
$$\langle W_\parallel\rangle = 1/2 \ kT_\parallel \tag{5.12}$$
$$\langle W_\perp\rangle = kT_\perp$$

Only the energy component in the direction of compression is affected by a compression. If the collision frequency is high enough to equalize $T_\parallel$ and $T_\perp$, then the system behaves three-dimensionally during any compression, and $\gamma = 5/3$. Toroidal plasma compression is illustrated in Fig. 5.5. Relations between dimensions and energies are summarized in Table 5.1.

Fig. 5.5 Top view of compression of a toroidal plasma **a** initial state, **b** after compression along minor radius a, and **c** after compression along major radius R
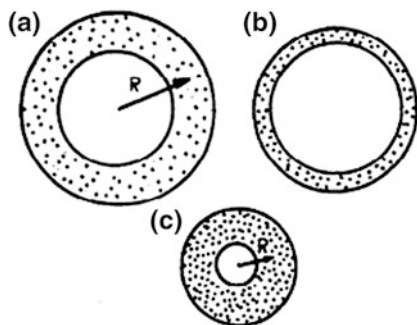

Table 5.1 Relation of energies to dimensions during adiabatic compression

Case	N	γ	Equation
Axial compression	1	3	$\langle W_\parallel\rangle L^2 = \text{constant}$
Compression along major radius	1	3	$\langle W_\parallel\rangle R^2 = \text{constant}$
Compression along minor radius	2	2	$\langle W_\perp\rangle a^2 = \text{constant}$
3-dimensional compression, or any compression in which a high collision rate makes the energy distribution isotropic	3	5/3	$\langle W\rangle V^{2/3} = \text{constant}$

In a *low-beta* plasma, the particles are tied to field lines, and

$$VB = \text{constant (radial compression)}$$
$$V/L = \text{constant (axial compression)} \tag{5.13}$$

where L = plasma length and B = magnetic field. (For a toroidal plasma L = $2\pi R_o$). For a *high-beta* plasma, the plasma pressure balances the magnetic field pressure:

$$2nT = \beta B^2/2\mu_o \tag{5.14}$$

$$TB^{-2}V^{-1} = \text{constant} \tag{5.15}$$

For a given change in B (or L) the change of volume may be computed from Eqs. (5.13) or (5.15), and then the corresponding energy change in the direction of compression may be computed from Eq. (5.11) or Table 5.1.

In tokamaks, conservation of toroidal flux requires that $B_t a^2 = $ constant. The toroidal field varies as $B_t = B_o R_o/R$. If B_o is not changed while the plasma is moved to smaller R, then

$$a^2/R = \text{constant} \tag{5.16}$$

Thus, a decrease of major radius with constant B_o also decreases the minor radius.

Example Problem 5.1: Adiabatic compression of a tokamak plasma A uniform tokamak plasma is compressed adiabatically (no heat loss) by using the vertical field to move the plasma from $R_o = 1.5$ m to $R = 1.0$ m without changing B_o. If the initial temperatures = 1 keV and density $n = 10^{19}$ m^{-3}, what are the final density and temperatures?

The compression of the major radius heats $T_{\parallel}$ according to the equation (Table 5.1)

$$\langle W_{\parallel} \rangle R^2 = \text{constant} \rightarrow T_{\parallel}/T_{\parallel_o} = \langle W_{\parallel} \rangle/\langle W_{\parallel_o} \rangle = R_o^2/R^2 = 2.25$$

So **T = 2.25 keV**.

The compression of the minor radius heats $T_{\perp}$ according to the equation (Table 5.1)

$$\langle W_{\perp} \rangle a^2 = \text{constant} \rightarrow T_{\perp}/T_{\perp o} = \langle W_{\perp} \rangle/\langle W_{\perp o} \rangle = a_o^2/a^2 = R_o/R = 1.5,$$

where Eq. (5.16) has been used. Thus, **$T_{\perp} = 1.5$ keV**.

The density change is

$$n/n_o = V_o/V = a_o^2 R_o/aR = R_o^2/R^2 = 2.25.$$

The final density is **n = 2.25 × 10^{19} m^{-3}**, assuming particle loss is negligible during compression.

If particles and energy are lost during compression, then the compression (no longer adiabatic) may be described using the transport equations.

Experiments with the Adiabatic Toroidal Compressor (ATC) tokamak demonstrated the effectiveness of this heating method. A tokamak could be compressed to ignition, and then allowed to expand with its temperature maintained by alpha heating. However, control of plasma size and shape is not easy, and pulsed coils present technological problems, such as fatigue.

Compression will not be used in tokamaks or stellarators, but it is the key feature of "magnetized target fusion" (MTF), where an imploding metallic liner compresses a "field reversed configuration" plasma up to high density and temperature.

5.5 Charged Particle Injection

5.5.1 Charged Particle Beams

It is difficult to inject charged particles across magnetic field lines, because the $q\mathbf{v} \times \mathbf{B}$ force reflects them. It is easy to inject them into a magnetic cusp or mirror along magnetic field lines, but they tend to follow field lines out the other end. The mean free path for Coulomb collisions is usually orders of magnitude larger than the size of the magnetic bottle, so Coulomb collisions are not effective in trapping the beam energy. However, microinstabilities, such as the beam-plasma instability, can extract beam energy over short distances and heat the plasma via wave-particle interactions.

Plasmas in magnetic mirrors have been heated to keV temperatures by axial injection of electron beams (Seidel 1979). Electron beams have also been injected into toruses, by varying the magnetic field during injection. Powerful electron and ion beams may also be used to compress solid fuel pellets in inertial confinement fusion experiments to very high temperatures and densities, resulting in small thermonuclear explosions.

5.5.2 Plasma Guns

A coaxial plasma gun is illustrated in Fig. 5.6.
When a high voltage is applied to the electrodes, breakdown occurs along the insulator. The $\mathbf{J} \times \mathbf{B}$ force accelerates the plasma outwards, then axially along the tube. Finally, the plasma momentum carries it off the end of the electrode as a blob of plasma moving along the chamber axis. Such plasma blobs, having keV temperatures, may be injected into plasma confinement systems. During injection

Fig. 5.6 Operation of a coaxial plasma gun **a** breakdown along the insulator, **b** acceleration of the plasma sheath, **c** continued acceleration past the end of the inner electrode, and **d** plasma blob leaving the end of the gun. The directions of plasma current density, self-magnetic field, and resultant $\mathbf{J} \times \mathbf{B}$ force are indicated at the *right*
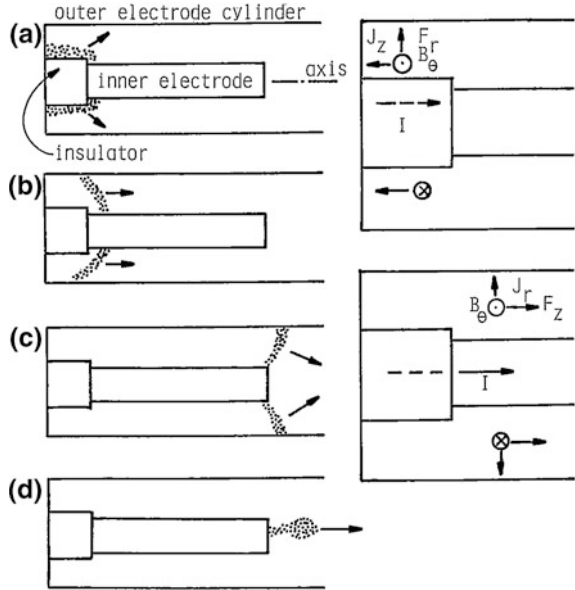
across B, the $q\mathbf{v} \times \mathbf{B}$ force produces a charge-separation electric field. This polarization field aids plasma penetration via the $\mathbf{E} \times \mathbf{B}/B^2$ drift.

A variation of the above method involves adding a solenoid inside the inner electrode. The solenoid field which connects the inner and outer electrodes gets stretched by the flowing plasma resulting in the generation of a spheromak in a formation chamber. A second electrical discharge with this spheromak accelerates it to high velocities through $J \times B$ forces.

Figure 5.7 shows a successful experiment that injected such plasma spheromaks from a magnetized coaxial plasma gun at $v = 2 \times 10^5$ m/s into the Tokamak de Varennes (TdeV) in Canada. For successful penetration, to first order, the kinetic energy density of the plasmoid must exceed the magnetic field energy density of the tokamak (Perkins et al. 1988).

The Mark III CT injector at 25 kV can inject compact toroids with density $\sim 7 \times 10^{21}$ m^{-3} at speeds ~ 200 km/s into the JFT-2 M Tokamak at the Japan Atomic Energy Research Institute (JAERI). These plasmas can also be injected into a spheromak flux conserver (Fukumoto et al. 2004).

Compact toroid injection may also be useful to inject fuel into the plasma core, which is desirable for plasma profile control and bootstrap current control (Sect. 7.4 and Raman 2006).

In some experiments the plasma blob leaving the end of a coaxial plasma gun collapses down to a very small diameter, *dense plasma focus*, which can be a source of intense neutron and x-ray emission. Such plasma focus devices have been constructed at many universities. Detailed photographs of the plasma sheath sometimes reveal tiny plasma vortex filaments (Bostick et al. 1966).
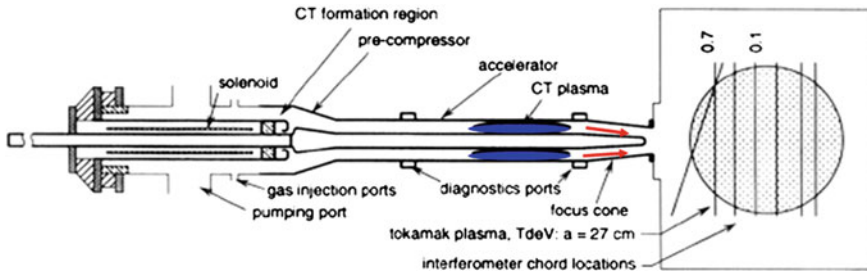
Fig. 5.7 The coaxial plasma gun used to inject plasma spheromaks into the TdeV experiment in Canada (Raman et al. 1994)

Another type of plasma gun uses a stack of titanium washers impregnated with deuterium. When a high current is pulsed through the stack, the deuterium is emitted, ionized, and accelerated.

Plasmas from guns also make good target plasmas for trapping injected neutral atom beams.

5.6 Neutral Beam Injection

5.6.1 Penetration into the Plasma

High velocity neutral atom beams can be injected across magnetic field lines and trapped in the plasma by ionization. If the plasma is not dense enough, most of the fast neutrals will pass through the plasma without being ionized. Conversely, if the plasma is too dense, or the beam energy is too low, most of the beam will be stopped at the plasma edge, without penetrating to the center where it is needed, Fig. 5.8.

The resultant density peak at the plasma edge may lead to instability. Thus, beam penetration and trapping requirements are relative to plasma density and beam energy. The unattenuated beam density $n_b(x)$ is trapped at a rate

$$dn_b/dx = -n_b/\lambda_a \tag{5.17}$$

where x is the distance of penetration measured from the plasma edge, and λ_a is the attenuation length. In a uniform plasma

$$n_b = n_{bo}\exp(-x/\lambda_a). \tag{5.18}$$

Values of the product $n_e\lambda_a$ for deuterium and tritium beams in a DT plasma are shown in Fig. 5.9 as functions of beam energy.

The ions trapped in distance dr at radius r will quickly spread out to fill the volume $(2\pi R_o)2\pi rdr$, for the case of circular flux surfaces in a torus with major radius R (Fig. 5.10).

Fig. 5.8 Beam penetration versus energy. The penetration distance also depends on plasma density
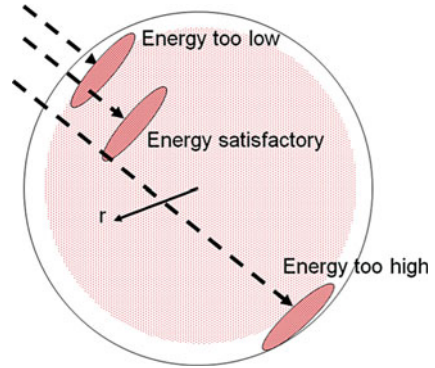

Fig. 5.9 Product of attenuation length λ_a and plasma density n_e versus neutral beam energy, for deuterium and tritium injection. *Smooth curves* $T_e = 10$ keV, *dashed curves* $T_e = 1$ keV (Dolan 1982)
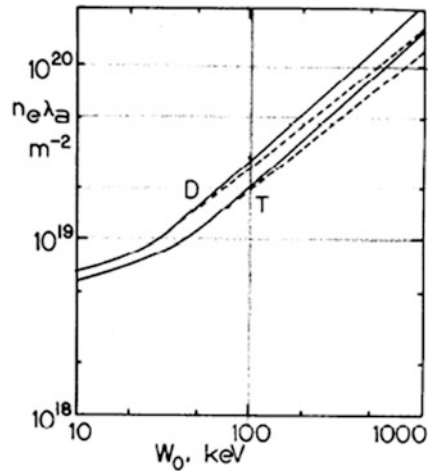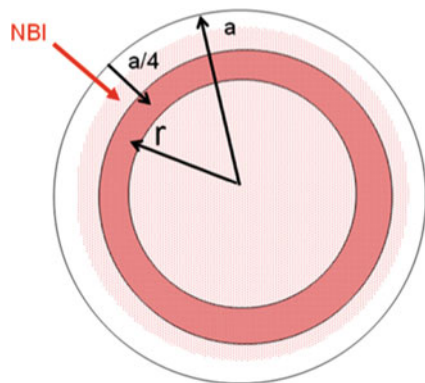

Fig. 5.10 Volume filled by trapped ions at radius r

This means that a few ions deposited at small r will provide a source density equal to that of many ions deposited at large r. If we let λ_{av} be the value of λ_a at the average values of n_e and T_e, then requiring that

Fig. 5.11 Variation of ion temperature with radius and time for an expanding radius tokamak reactor case. Neutral beam heating is turned on from t = 2–6 s, with radius a = 1.4 m. Then the plasma becomes ignited and is allowed to expand to a = 2.5 m, with T_i sustained by alpha heating (Houlberg et al. 1980)
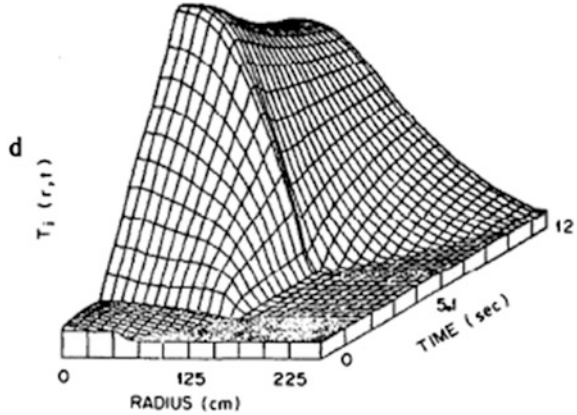
$$\lambda_{av} > a/4 \qquad\qquad (5.19)$$

may give adequate penetration. For example, consider a case in which the average electron density $n_e = 8 \times 10^{19}$ m^{-3}, a = 1.25 m. For this case $n_e a = 10^{20}$ m^{-2}. To attain $n_e \lambda_{av} > 2.5 \times 10^{19}$ m^{-2}, the desired deuterium atom beam energy is about 100 keV.

It is possible to ignite large reactor plasmas without using much higher beam energies by keeping the plasma radius small until neutral beam heating has ignited the plasma, then allowing the plasma to expand to full size. For example, a tokamak reactor case with the following parameters was studied:

$R_o = 10$ m, $B_t = 4.2$ T, plasma elongation (height/width) = 1.6, initial minor radius a = 1.4 m, $n_e = 10^{20}$ m^{-3}, neutral beam energy = 150 keV, beam power = 130 MW, heating pulse length = 4 s, initial plasma current = 3 MA; final expanded radius a = 2.5 m, final current I = 8 MA. The time variation of the ion temperature profiles for this case is shown in Fig. 5.11.

These data illustrate the type of calculations needed for neutral beam energy deposition studies. They are not conclusive, because the results depend strongly on

- Transport model assumed
- Alpha particle confinement
- Alpha energy transfer to electrons and ions.

Small ripples in the toroidal field ($\delta B_t/B_t \sim 1$ %) may help transport trapped ions inwards, permitting somewhat lower injection energies to be used, if instabilities do not interfere.

5.6.2 Neutral Beam Generation

Neutral atoms cannot be accelerated, since they are not much affected by electromagnetic fields. However, ion beams can be accelerated and then partially

Fig. 5.12 The steps of neutral beam generation and injection
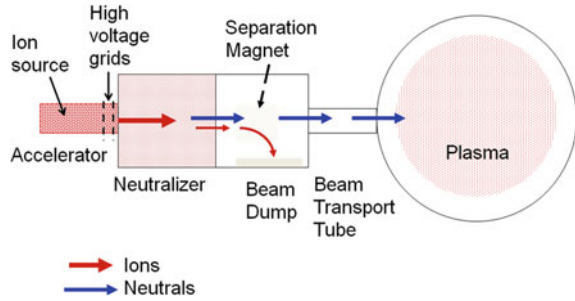
neutralized by charge transfer in a gas cell. Figure 5.12 illustrates the steps of neutral beam generation.

Hydrogen ions from an ion source are accelerated by high voltage grids. The ion beam passes through a neutralizer cell, which may contain a gas like deuterium or nitrogen. Part of the ions grab electrons and become neutral atoms that are not affected by the magnetic field of the separation magnet. The part of the beam that is not neutralized is deflected by a separation magnet into a beam dump, so that it does not hit the walls of the beam transport tube.

Figure 5.13 shows more details, including Doppler shift spectroscopy to measure neutral atom velocities.

5.6.2.1 Need for Negative Ions

The D_2 gas pressure in the neutralizer region is on the order of 0.1 Pa (10^{-3} Torr). The fraction of the ion beam neutralized by charge exchange is
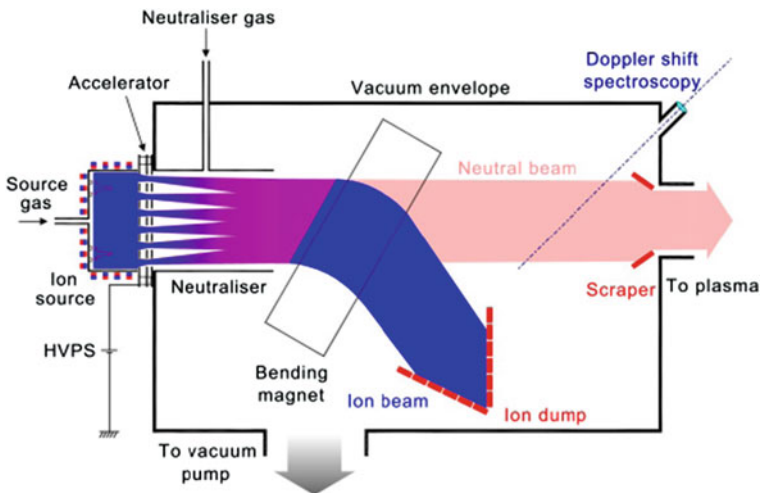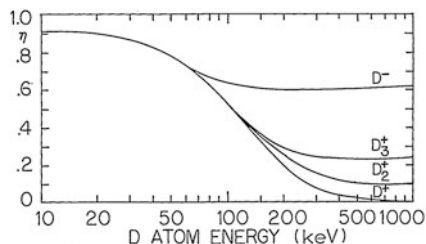

Fig. 5.13 The main components of a neutral beam injector (Day et al. 2010). Used by permission of United Kingdom Atomic Energy Authority

Fig. 5.14 Neutralization efficiency η versus beam energy for deuteron beams in deuterium gas (Dolan 1982)

$$\eta = \frac{\sigma_{10}}{\sigma_{10} + \sigma_{01}} \left\{ 1 - \exp\left[-(\sigma_{10} + \sigma_{01}) \int_0^x dx\, n_n \right] \right\} \qquad (5.20)$$

where x is the path length in the gas, n_n is the gas density, σ_{10} is the cross section for neutralization by charge exchange, and σ_{01} is the cross section for reionization of the neutrals. For values of

$$\int_0^x dx\, n_n \geq 2 \times 10^{20}\,\mathrm{m}^{-2}, \qquad (5.21)$$

the exponential function is very small, and

$$\eta \cong \sigma_{10}/(\sigma_{10} + \sigma_{01}). \qquad (5.22)$$

Since σ_{10} drops off at high energies, the neutralization of positive ions becomes inefficient there, as shown in Fig. 5.14.

The rapid drop of the D+ curve means that efficiency will be poor for neutralization of D+ beams above 200 keV. Negative ion (D$^-$) beam sources are being developed for production of high-energy neutral beams, because such beams have much higher neutralization efficiencies than D+ beams. 1 MeV negative ion sources have been developed for ITER. Direct recovery of unneutralized ion energy in the beam dump can improve the power efficiency of neutral beam production.

Negative ions can be generated by contact with a low-work-function surface (such as Cesium) and by dissociative recombination of a vibrationally excited molecule, such as D_2^* (energy levels $\sim$ 5–10)

$$D_2^* + e^- \rightarrow D_2^{-*} \rightarrow D^- + D^o$$
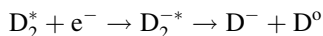
5.6.3 Ion Sources

The ion source needs to provide a large uniform plasma. One way to do this is with permanent magnet multipole cusp arrangement, as illustrated in Fig. 5.15.
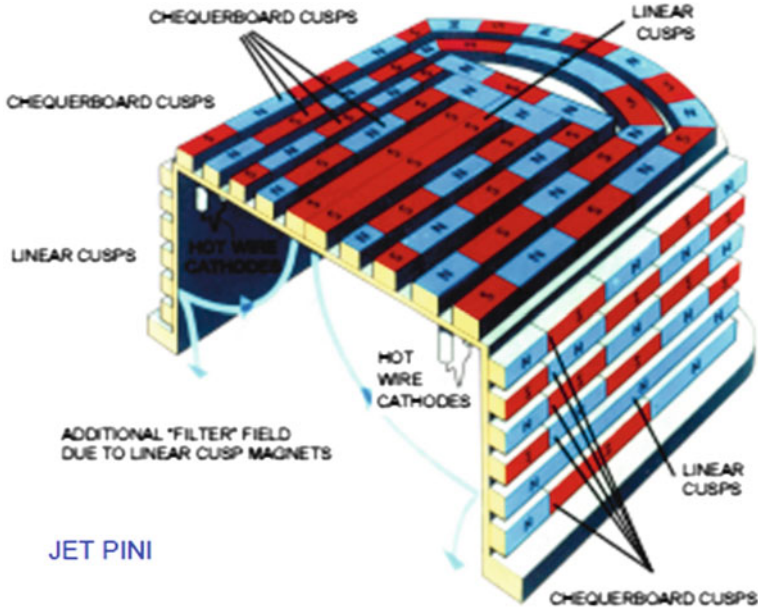
Fig. 5.15 The JET PINI multipole cusp ion source (Day et al. 2010). Used by permission of United Kingdom Atomic Energy Authority

The magnetic field provides thermal insulation at the wall, and the weak field in most of the volume allows the plasma to be uniform. Figure 5.16 shows an expansion region between the ion source and the accelerating grids.

Fig. 5.16 Plasma expansion up to the accelerating grids. The magnetic field filters out electrons (Day et al. 2010). Used by permission of United Kingdom Atomic Energy Authority
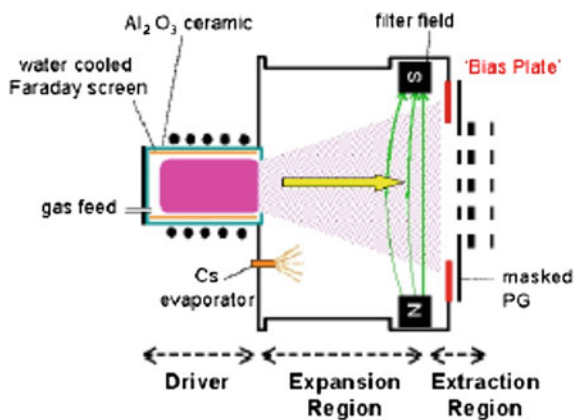
Fig. 5.17 Accelerating
electrodes (*black*), magnetic
fields (*red*), and beam (*blue*)
(Day et al. 2010). Used by
permission of United
Kingdom Atomic Energy
Authority

-130kV   -110kV   0

Plasma   Electron   Ground
grid   trap   grid
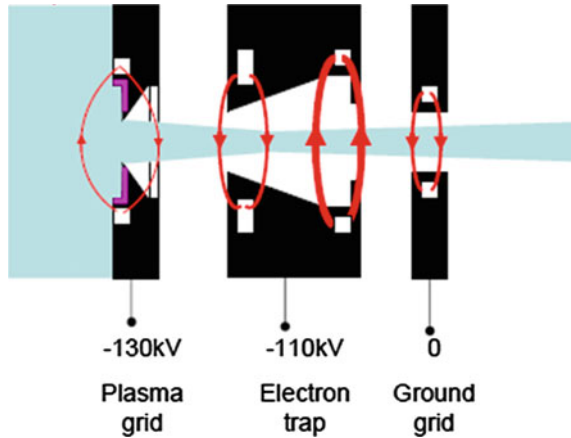
5.6.4 Accelerator

Beam divergence is typically about half a degree in the plane parallel to the electrode slits and 1.3° in the plane perpendicular to the electrodes (at 37 % of peak intensity). Grid rails are fastened at one end only, to allow for thermal expansion, and the grids (usually copper) are water-cooled. Current densities attainable by ion beam sources are typically around 3 kA/m^2 (0.3 A/cm^2). A grid misalignment of just 0.1 mm can cause a beam deviation of 3.6 cm after 8 m travel to the torus.

Figure 5.17 shows a set of accelerating electrodes for negative ion acceleration.

The magnetic fields help trap co-injected electrons, so that energy is not wasted accelerating them. The electron current can also be reduced by positively biasing the area around the aperture (Day et al. 2010).

Multiple aperture electrodes will accelerate many beamlets, over 1,000 each in JT-60U and ITER.

In the event of sparking, the high voltage must be rapidly disconnected to prevent arc damage to the electrodes.

5.6.5 Beam Duct and Pumping

Figure 5.18 shows how several neutralized beams merge as they pass through the JET beam duct into the torus.

The cryogenic vacuum pumping system must remove most of the neutral gas, to prevent it from flowing into the plasma region. A fast shutter valve can be closed after the end of the beam pulse to prevent further gas flow, if needed, and to facilitate glow discharge cleaning between plasma discharges. The entire injector may be pivoted around flexible bellows to vary the injection angle. Buildup of neutral gas in the beam duct during injection may cause reionization of the beam and prevent its penetration across the magnetic field.
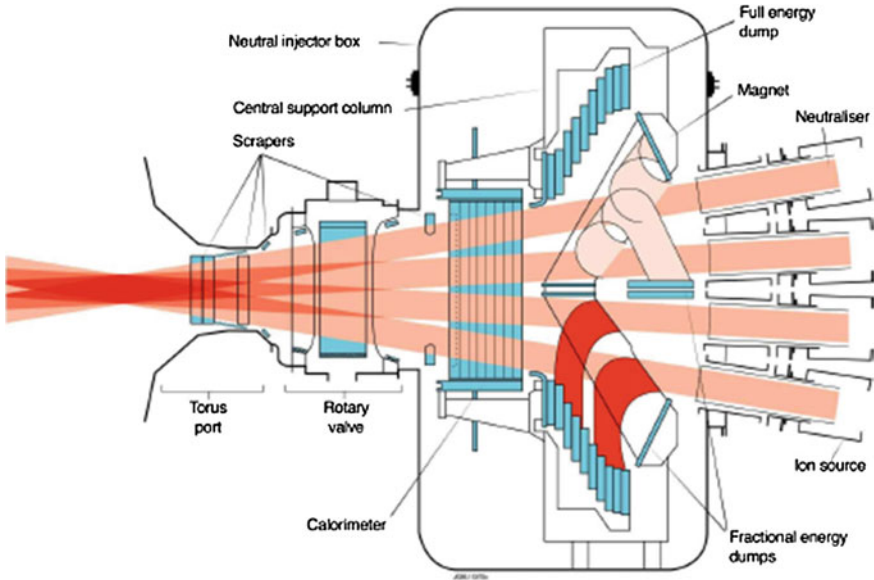
Fig. 5.18 Convergence of several neutral beams as they pass through the beam duct into JET (Day et al. 2010). Used by permission of United Kingdom Atomic Energy Authority

In order to prevent reionization from spoiling beam heating, the parameter $P_o t \ell / C$ should be minimized, where P_o is the desired beam power of primary D^o, t is the pulse length, R is the duct length, and C is the conductance of the vacuum system for deuterium leaving the beam duct. Large cryogenic pumps with surfaces at $T \sim 5$ K must provide very high vacuum pumping speeds for many minutes in ITER. Vacuum pumps will be discussed in Sect. 9.3.

Some design considerations for neutral beam injectors are listed in Table 5.2 (There are also many other considerations related to mechanical design, vacuum system, cryogenics system, magnet system, and electrical systems).

Table 5.3 lists the ITER NBI systems.

Experimental injectors have achieved the desired values of current density (200 A/m^2), (electron/ion) ratio (<1), and operating pressure (0.3 Pa). Full power capability for 3,600 s is under development.

Figure 5.19 shows the ITER neutral beam injector system.

This system has a source of D^- negative ions that are accelerated up to 1 MeV and then neutralized. The vertical bushing provides high voltage insulation. The injected beam power is 1 MW, and the beam must perform reliably for many seconds. The fast shutter closes when the beam is not being injected to keep unwanted gas from streaming into the tokamak. The calorimeter is used to measure beam power.

Two heating Neutral Beam Injectors (HNB) are currently foreseen for ITER with a possible third, plus a Neutral Beam for diagnostic purposes (DNB). A preliminary idea of their locations around the torus are shown in Fig. 5.20.

Table 5.2 Some neutral beam injection design considerations

- Long pulse duration
- Negative ion beams at high energies
- Current density—need narrow electrode gaps and high voltage
- High voltage breakdown—desire large gaps and smooth surfaces
- Beam divergence angle—computerized electrode design
- Beam blowup—narrow beamlets, electrode thermal expansion allowance
- Overheating—flowing water or helium
- Arc damage—fast-cutoff circuitry
- Electrode sputtering—low neutral gas pressure
- Radiation damage—electrodes shielded from neutron flow paths
- Gas flow—powerful cryogenic vacuum pumps
- Efficiency—recover un-neutralized ion beam energy at beam dump

Table 5.3 ITER NBI system plans

	Energy	Power
Heating and current drive	1 MeV	2×16.5 MW, 3,600 s
Diagnostics	100 keV	6 MW
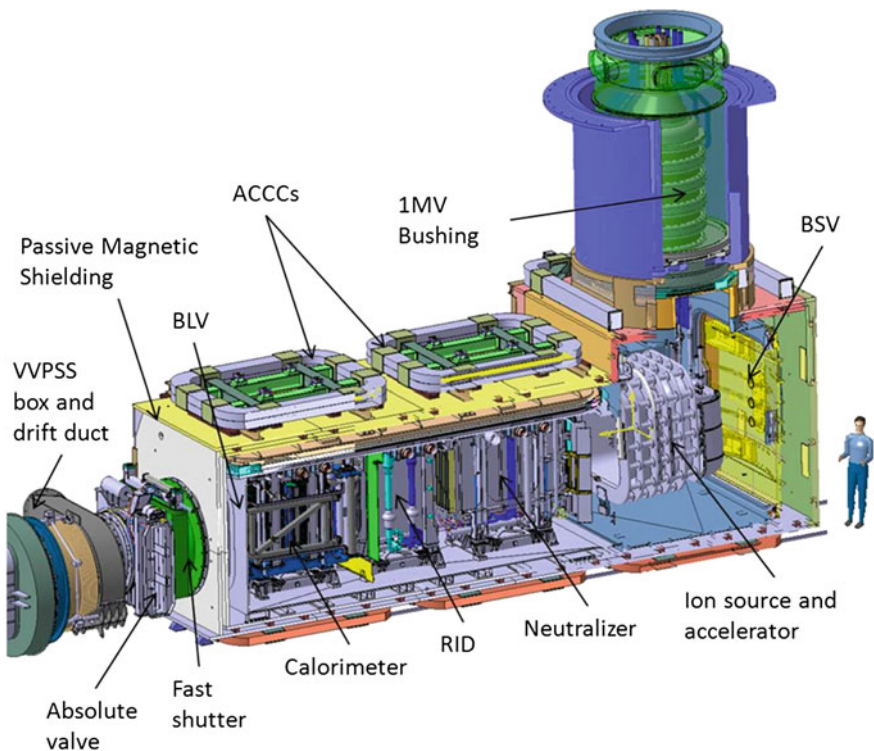
Fig. 5.19 The ITER neutral beam injector. Courtesy of ITER Organization
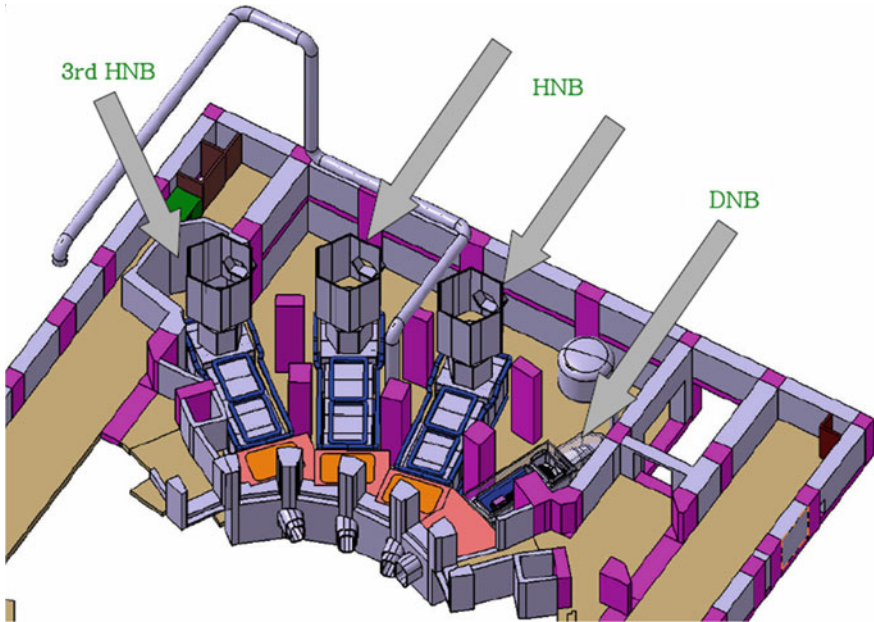
Fig. 5.20 A preliminary concept for arrangement of neutral beam injectors (Design is evolving). Courtesy of ITER Organization

5.7 Wave Heating Fundamentals

5.7.1 Electromagnetic Waves

Plasma may be heated with various forms of electromagnetic waves, including radio waves, microwaves, and laser beams. Laser beams may be used to heat high density plasma ($n > 10^{23}$ m^{-3}) and to compress solid fuel pellets, but absorption of laser light is ineffective at lower plasma densities, as in tokamaks ($n \sim 10^{20}$ m^{-3}).

Electromagnetic waves are represented in terms of their angular frequency ω (radians/s) and wave vector **k,** which has a magnitude $= 2\pi/\lambda$ (λ = wavelength) and direction equal to the direction of wave propagation. The frequency f in Hz (cycles/s) $= \omega/2\pi$. The wave frequency is fixed by the generator, and the wavelength depends on the response of the plasma. In a vacuum

$$\lambda = c/f \qquad (5.23)$$

where c = speed of light. The wave vector **k** has components $k_\parallel$ parallel and $k_\perp$ perpendicular to the magnetic field direction. The electric field of each wave varies sinusoidally with space and time according to:

$$E = E_o \exp(i\mathbf{k} \cdot \mathbf{x} - i\omega) \qquad (5.24)$$

(which can also be written in terms of sines and cosines). There will be many such waves in the plasma simultaneously with various $\mathbf{k}$ and ω, so the total electric field is the sum of all the individual wave electric fields. The phase velocity and "group velocity" v_g of the wave are

$$
\begin{aligned}
v_{ph} &= \omega/k \\
v_g &= \partial\omega/\partial k
\end{aligned}
\qquad (5.25)
$$

The wave fields travel at v_{ph}, which can exceed the speed of light c, but energy and information travel at v_g, which is always <c. These can be seen from the ratio of ω/k and from the slope of a graph of ω versus k. To study plasma waves we assume that the plasma density has a large constant part n_o and a small part n_1 that varies exponentially at the wave frequency

$$n = n_o + n_1 \exp(i\mathbf{k} \cdot \mathbf{x} - i\omega t) \qquad (5.26)$$

We make similar assumptions about other plasma quantities and insert these approximations into the conservation equations and Maxwell equations. The goal is to derive a "dispersion relation" (an equation that relates $\mathbf{k}$ to ω). Then we can analyze that equation to study the wave propagation.

Figure 5.21 shows graphs of the dispersion relations for waves propagating parallel to B and perpendicular to B in a "cold plasma" (meaning that plasma temperature and pressure effects are ignored).

The slopes of these curves are the group velocities, always less steep than the dashed line c. We can identify resonances that may be useful for plasma heating or current drive: electron cyclotron resonance (ECR), ion cyclotron resonance (ICR), upper hybrid resonance (UHR), and lower hybrid resonance (LHR). We can also heat the plasma at twice the ECR and ICR frequencies (the "second harmonic") or even higher harmonics, though perhaps less effectively. In general the wave propagates at an intermediate angle relative to B, so these are special, simplified cases.

The Index of Refraction

$$N = c/v_{ph} = kc/\omega \qquad (5.27)$$

can vary between 0 and infinity. (When $N < 1$, $v_{ph} > c$.) The variation of the wavelength in a plasma approaching a cutoff and a resonance is shown in Fig. 5.22.

5.7.2 Stages of Wave Heating

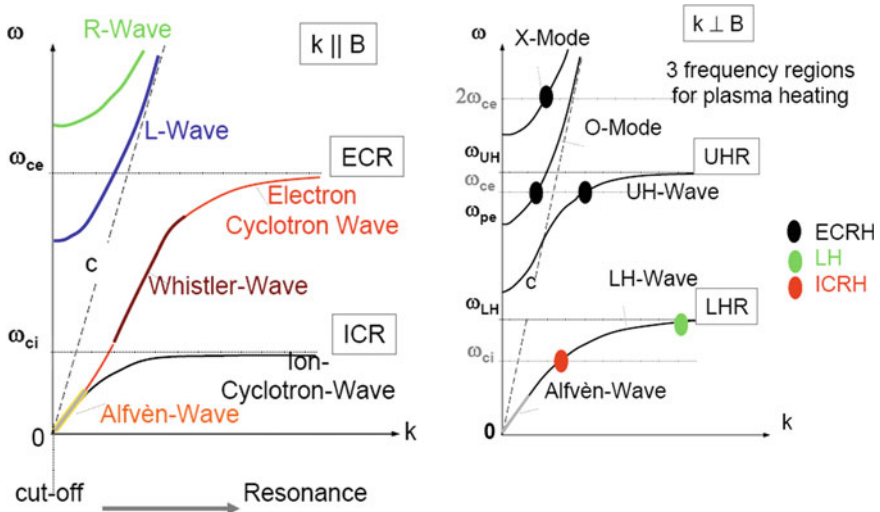The stages of electromagnetic wave heating are illustrated in Fig. 5.23.

Fig. 5.21 Dispersion relations for electromagnetic waves propagating parallel to B and perpendicular to B in a "cold plasma". The places where k → ∞ (v_{ph} → 0) are "resonances" where the plasma absorbs the wave energy, and the places where k → 0 (v_{ph} → ∞) are "cutoffs", where the wave cannot propagate (it may be reflected or modified into a different wave) (Laqua 2008)
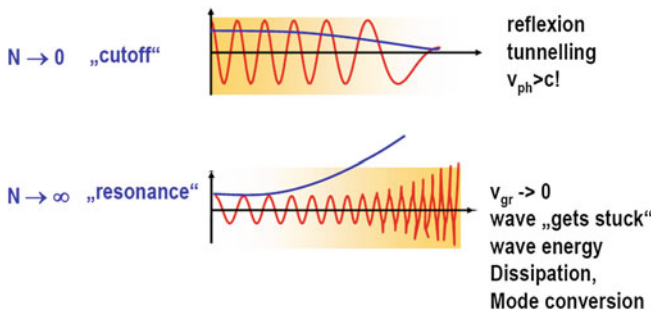

Fig. 5.22 Variation of wavelength as the wave approaches a cutoff and a resonance. The *blue curve* shows how N varies near the cutoff and resonance. Near the cutoff λ → ∞ (k → 0), and near the resonance λ → 0 (k → ∞) (Laqua 2008)

The problems of generation and transmission are fairly well resolved, except for high power generation of waves at frequencies >100 GHz. Coupling is most effective near resonances of the plasma or near resonant frequencies of the plasma-filled chamber.

A vacuum window is usually needed between a microwave generator and the plasma. It should have low absorption of the waves, high thermal conductivity, and resistance against cracking at high power densities of waves passing through. Diamond and sapphire are excellent materials, because of their high thermal

Fig. 5.23 Stages of wave heating (Stix 1972)
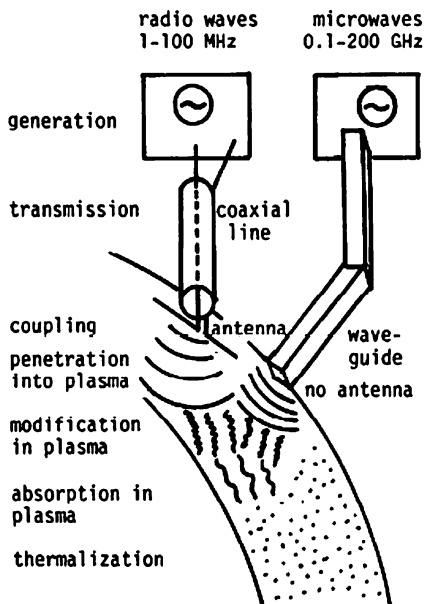
conductivities, but expensive. The waveguide should have several bends in it to prevent neutrons from streaming to the outside and causing high radiation levels outside the reactor.

Radio waves are transmitted through coaxial lines, and microwaves usually travel through rectangular waveguides. Special dielectric-filled or convoluted waveguides may be used where the wavelength is large.

A waveguide grill couples microwaves to the plasma, and an antenna is used for radiofrequency waves. Antennas must couple efficiently, without arcing or intro-ducing impurities into the plasma. For all types of heating, the antenna structure or waveguide array should be arranged so as to excite desired modes in the plasma. Otherwise, coupling may be inefficient, and required antenna voltages may become excessive, or waves may merely heat the surface plasma without pene-trating to the core.

The physics of wave-plasma interactions are described in plasma physics textbooks (Chen 1984; Kikuchi et al. 2012; Stix 1972). Penetration into the plasma depends upon the relation of the wave frequency and wave number $k = 2\pi/\lambda$ to the local plasma properties. The wave may be reflected by the plasma, which prevents effective heating or current drive. It may pass through the plasma with little interaction. It may change into other wave forms inside the plasma, and part of the wave energy may be absorbed by the plasma. Computer programs model the wave propagation and interaction in the plasma to predict the effectiveness of heating and current drive.

Absorption is strongest at natural resonances of the plasma, which include the electron cyclotron, ion cyclotron, lower hybrid, and upper hybrid resonances. Absorption could also be enhanced by resonances of the "cavity" (chamber).

Fig. 5.24 Multiple
reflections of wave in a cavity
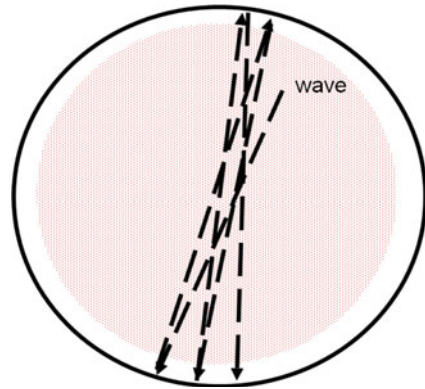
5.7.3 Cavity Resonances

Cavity resonances of electromagnetic waves, similar to those of sound waves in a
musical instrument, can occur when the size of the cavity (in this case, the vacuum
vessel) is an integral number of half-wavelengths. An electromagnetic wave that is
weakly absorbed by plasma can pass through the plasma many times, reflecting
from the vacuum chamber walls, Fig. 5.24.

If the wave frequency is tuned to one of the natural resonant frequencies of the
plasma-filled cavity, then the wave amplitude in the plasma can become very large
(limited by the reflectivity of the walls and by wave absorption in the plasma),
resulting in effective plasma heating in spite of the weak absorption.

Changes of the plasma density profile alter the resonant frequencies of a cavity.
For effective plasma heating, the radio wave generator frequency must follow the
resonant frequency of the cavity and plasma. This frequency variation is called
mode tracking. Usually the impedance of the plasma and chamber is low compared
to that of the radio wave transmission system and antenna. The impedance mis-
match may result in ineffective coupling of the wave energy to the plasma. Near a
resonance, the plasma impedance increases, and coupling becomes more efficient.
In the 1960s resonant cavities were studied as a possible means of *confining* a fusion
plasma, but the input power requirements were too high (Dolan 1982, Chap. 17).

5.7.4 Propagation and Resonances

Electromagnetic waves propagating perpendicular to the magnetic field have two
basic modes: the "ordinary mode" (E parallel to B) and the "extraordinary mode"
(E perpendicular to B). Usually E will have components both parallel and per-
pendicular to B. These modes have different propagation characteristics. The
direction of E can be controlled by the orientation of E in the waveguide or

antenna leading to the plasma. The ordinary mode wave will be reflected at the plasma layer where the wave frequency ω = the electron plasma frequency

$$\omega = \omega_{pe} = (ne^2/m_e\varepsilon_o)^{1/2} = 56.4 \ n^{1/2} \ \text{rad/s} \tag{5.28}$$

where n = electron density (m^{-3}). For example, if n = 10^{20} m^{-3}, then ω_{pe} = 56.4×10^{10}, and $f_{pe} = \omega_{pe}/2\pi$ = 90 GHz, so only very high microwave frequencies could penetrate.

The extraordinary mode can penetrate further, but propagation of the waves is complicated, because they can interact with various other waves and resonances in the plasma (Bellan 2006; Chen 1984; Goldston and Rutherford 1995; Kikuchi et al. 2012; Stix 1992) Here we will look at some of the hardware used to generate, transmit, and couple the waves to the plasma.

The plasma has several resonant frequencies at which the wave energy may be readily absorbed:

Electron cyclotron resonance heating (ECRH or ECH or EC)

$$\omega_{ce} = eB/m_e\gamma \qquad \text{rad/s} \tag{5.29}$$

where e = electron charge, B = magnetic field, m_e = electron mass, $\gamma = (1 - v^2/c^2)^{1/2}$ (same as Eq. 2.12. We assume $\gamma = 1$ unless otherwise specified.). The frequency in Hertz is

$$f_{ce} = \omega_{ce}/2\pi = 28.0 \, B \ \text{(GHz)} \tag{5.30}$$

Ion cyclotron resonance heating (ICRH or ICH or IC)

$$\omega_{ci} = qB/m_i \ \text{rad/s} \tag{5.31}$$

where q = ionic charge, B = magnetic field, m_i = ion mass. The frequency in Hertz is

$$f_{ci} = \omega_{ci}/2\pi \ \text{Hz} \tag{5.32}$$

For deuterons this becomes

$$f_{ci} = 7.63 B \ \text{MHz} \tag{5.33}$$

At B = 5 T this becomes 38 MHz, which corresponds to a vacuum wavelength of 7.9 m. The ITER ion cyclotron heating system uses radio waves at frequencies of 30–50 MHz.

Lower hybrid resonance (LH)

The lower hybrid resonance frequency is

$$\omega_{LH} \simeq \omega_{pi}(1 + \omega_{pe}^2/\omega_{ce}^2)^{-\frac{1}{2}} \ \text{rad/s} \tag{5.34}$$

where $\omega_{pi} = (ne^2/m_i\varepsilon_o)^{1/2}$ and $\omega_{pe} = (ne^2/m_e\varepsilon_o)^{1/2}$ are the ion plasma frequency and electron plasma frequency, and m_i and m_e are the ion and electron masses. The frequency $f_{LH} = \omega_{LH}/2\pi$ is typically a few GHz.

Table 5.4 Some wave heating methods and ITER plans (partly from Jacquinot et al. 2008)

	IC	LH	EC
Frequency in ITER	35–65 MHz	3.7–5 GHz	170 GHz
Objectives in ITER	Central ion heating; sawtooth control; wall cleaning	Off-axis current drive	Heating; current drive; NTM[a] control; plasma startup
CW power to ITER plasma (MW)	20	20	20
Transmission means	Coaxial line	Waveguide	Waveguide
Coupling means	Loop antenna or cavity-backed aperture antenna	Waveguide array with specified phases	Waveguide array
Generation efficiency (%)	70	60	55
Performance achieved in 2008	22 MW/3 s	3 MW/360 s	1 MW/800 s

[a] *NTM* neoclassical tearing modes

Upper hybrid resonance

The upper hybrid resonance frequency is

$$\omega_U \equiv (\omega_{pe}^2 + \omega_{ce}^2)^{\frac{1}{2}} \qquad (5.35)$$

This frequency is used less than other resonances, because it is very high.

For example, in a deuterium plasma with $n = 10^{20}$ m^{-3} and B = 5 T, these frequencies are $f_{ce} = 140$ GHz, $f_{ci} = 38$ MHz, $f_{LH} = 1.25$ GHz, and $f_U = 166$ GHz.

Electromagnetic waves may undergo mode conversion (transformation to another type of plasma wave) in the plasma. The wave energy may be absorbed by Landau damping (in which particles gain energy from the wave, like a surfer on an ocean wave) or other processes. Then collisions between particles thermalize the energy, raising the plasma temperature.

Examples of wave heating systems applicable to ITER are listed in Table 5.4.

Wave heating methods are discussed by Wesson (2011) and by Kikuchi et al. (2012).

5.8 Ion Cyclotron Resonance Heating

The Ion Cyclotron Resonance Heating (ICRH) method is also called "Ion cyclotron range of frequencies" (ICRF), since the frequencies used may vary from the exact cyclotron frequency.
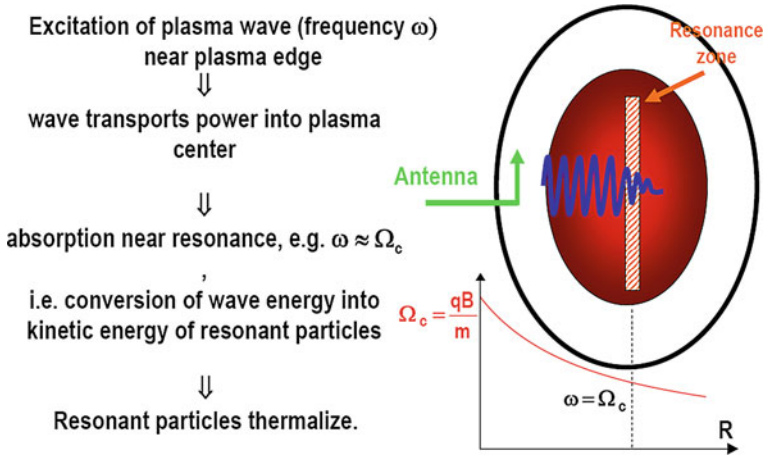
Fig. 5.25 Location of resonance zone at a specific magnetic field and radius R (Laqua 2008)

Based on Eq. (2.8) the toroidal magnetic field in a tokamak varies as

$$B(R) = B_o R_o / R \qquad (5.36)$$

where B_o is the magnetic field at the plasma axis R_o. Each value of radius has a value of B corresponding to a specific cyclotron resonance frequency. By choosing the generator frequency we can choose the radius where the ion cyclotron resonance occurs, hence the radius where the ICR heating occurs. Other resonances, like ECR, can also be aligned to specific plasma locations. This is illustrated in Fig. 5.25.

5.8.1 Propagation and Coupling

There are two modes of propagation: the "slow wave" and the "fast wave". The slow wave requires a complex antenna to facilitate launching and penetration. The fast wave decays as $\exp(-2\,k_\parallel\,x)$, where x is the distance from the antenna to the cutoff layer and $k_\parallel$ is the parallel wave number component parallel to the magnetic field. If the antenna size is $>4\pi x$, then most of the wave energy penetrates through the cutoff layer (Sheffield 1994).

If several percent of protons are present in a deuterium plasma, these protons can absorb the heating at their cyclotron frequency and transfer it collisionally to the deuterons and electrons. ^{3}He ions are also used for this "minority heating" process. At higher minority concentrations part of the wave energy may be coupled to Bernstein electrostatic waves and absorbed by collisionless Landau damping (Wesson 2011).

Wave energy can also be absorbed at harmonics of ω_{ci} (ω_{ci}, $2\omega_{ci}$, $3\omega_{ci}$, …). Second harmonic heating can yield temperatures >10 keV in large tokamaks.
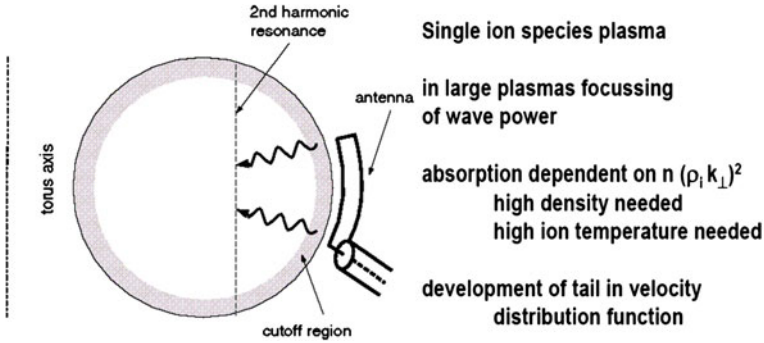
Fig. 5.26 Second harmonic ICRH in ITER. Here ρ_i represents the ion cyclotron radius (Laqua 2008)

High voltage breakdown must be avoided in the transmission line, vacuum window, and antenna. The radiofrequency voltages expected at high power are on the order of 30 kV. Cool plasma near the antenna may short out the antenna voltage, and arcs may develop at joints, windows, in waveguides, etc. The generators must be rapidly switched off if an arc persists for more than one cycle, to avoid damage to equipment. In a reactor environment, radiation damage to rf antennas may be severe.

One heating method in ITER can be at the ion cyclotron resonance second harmonic, as shown in Fig. 5.26.

5.8.2 ICRF Generators and Transmission Lines

A 2 MW radiofrequency generator is shown in Fig. 5.27.

Figure 5.28 shows the ASDEX Upgrade power transport system with large coaxial transmission lines. The matching network needs to adjust the wave phase in order to minimize reflection and losses along the transmission line and to try to match the impedance to the load.

The Tore Supra tokamak (R = 2.4 m, a = 0.8 m, B = 4.5 T) has sustained 1 MA plasma current for 30 s using 6 MW ICRH plus 3.4 MW LHCD (Bucalossi 2010).

5.8.3 Antennas

A widely used antenna design is a strap antenna behind a Faraday cage screen, Fig. 5.29. Radiofrequency current oscillates back and forth in the strap antenna, inducing an electromagnetic wave that propagates towards the plasma. The Faraday screen helps separate the high electric field of the antenna from the plasma, reducing
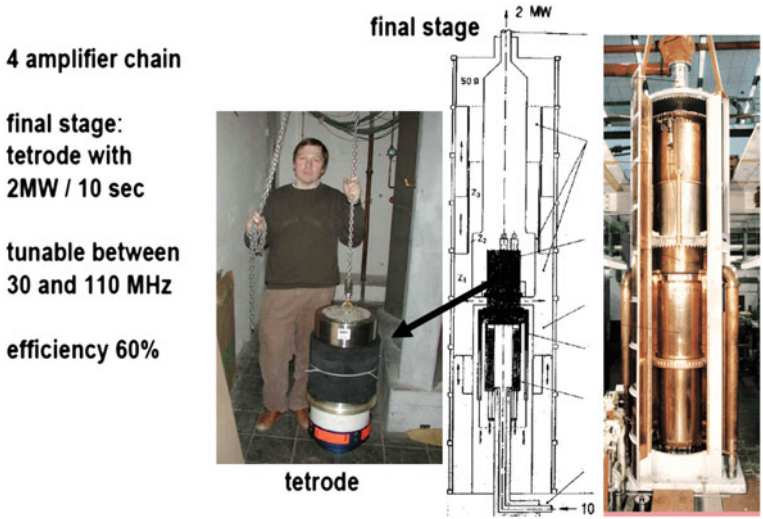
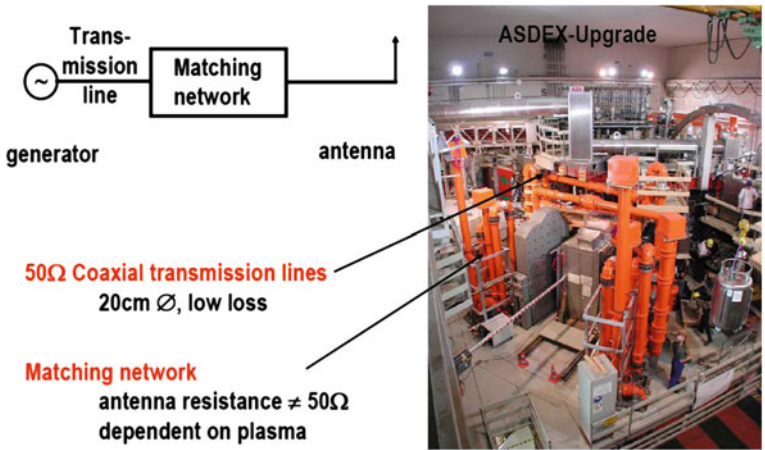**Fig. 5.27** A 2 MW tetrode generator for ICRH (Laqua 2008)

Fig. 5.28 The ITER ICRH power transport system (Laqua 2008)

arcing and sputtering. The antenna must be close to the plasma, because there is usually a thin "cutoff" region near the wall through which wave penetration is difficult. Close to the antenna the fields are stronger and penetration is more probable, but sputtered impurities from the antenna can cause problems, such as arcing.

The ITER ICRH antenna system is shown in Fig. 5.30.

This is similar to the antenna of the Joint European Torus (JET), Fig. 5.31.

The impedances of the coaxial lines and antennas are carefully designed to minimize power losses and to maximize the efficiency of energy transfer to the plasma.
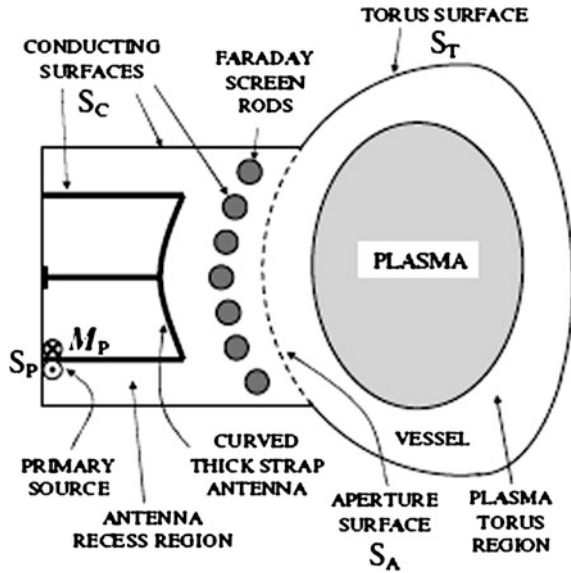
Fig. 5.29 Schematic sectional view of a typical ICRF antenna (Lancellotti et al. 2006, Fig. 1)
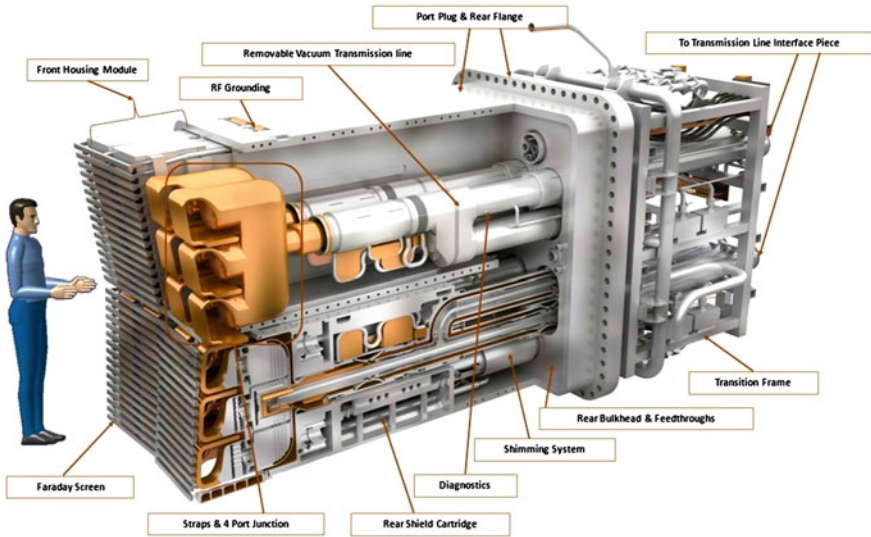

Fig. 5.30 The ITER ion cyclotron resonance heating and current drive antenna. Courtesy of ITER Organization
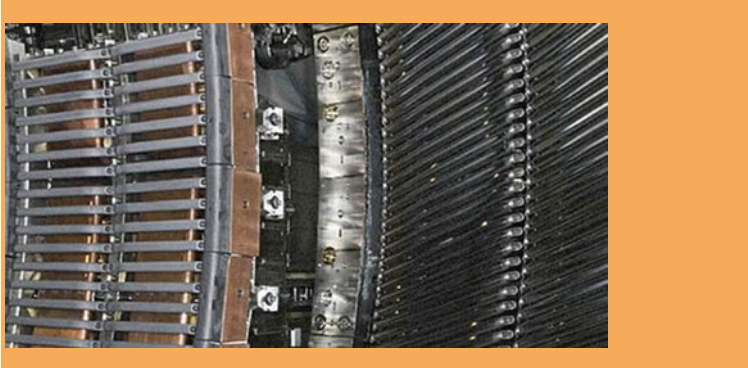
Fig. 5.31 Ion cyclotron antennae at JET. *Vertical* copper straps are visible behind the *horizontal* Faraday screen bars. Image supplied courtesy of Culham Publication Services, copyright EURATOM

A study of tungsten sputtering from ICRF antennas in ASDEX-Upgrade finds that the sputtering can be reduced by

- Increasing plasma–antenna clearance;
- Strong gas puffing;
- Decreasing the intrinsic light impurity content (mainly oxygen and carbon);
- Extending the antenna box and structures parallel to the magnetic field;
- Increasing the number of toroidally distributed straps;
- Better balance of (0π)-phased contributions to RF image currents (Bobkov et al. 2010).

Studies of ICRF antenna designs aim to reduce the rf sheath potential and sputtering of the antenna surface, which shortens its lifetime and adds impurities to the plasma (Mendes et al. 2010). The ITER ICRH antenna designs are being studied with complex computer models (Messiaen et al. 2010; Milanesio et al. 2010).

Heating and current drive with the "high harmonic fast wave" in the National Spherical Torus Experiment (NSTX) were improved when the plasma density was reduced near the antenna, such as by coating nearby vessel surfaces with lithium to reduce plasma density near the antenna (Phillips et al. 2009; Taylor et al. 2010).

ICRH waves can provide strong central heating with high efficiency and low cost, but their use for current drive is less promising.

5.9 Electron Cyclotron Heating

5.9.1 Wave Propagation

By adjusting the wave frequency to a specific magnetic field value, the Electron Cyclotron Heating (ECH) system can deposit energy at a specified radius R. This
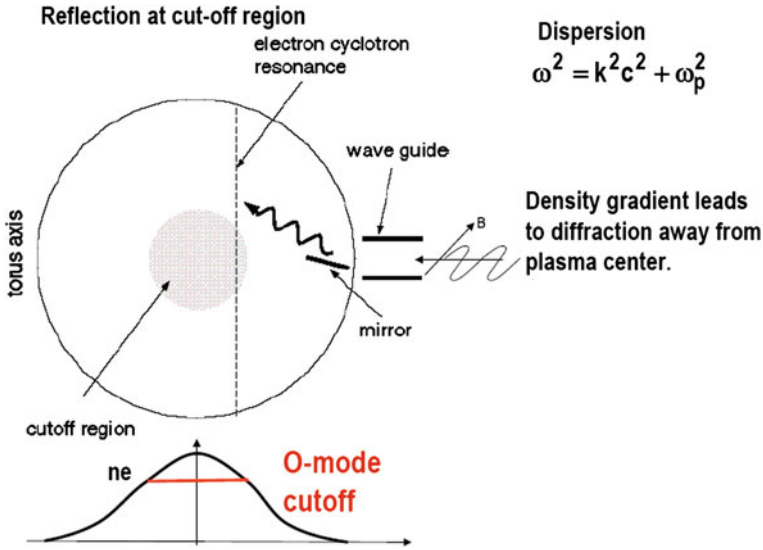
Fig. 5.32 Cutoff of the O-mode in the high density region (Laqua 2008)

spatial selectivity helps control the plasma profiles and current drive, which can help maintain good plasma stability and energy confinement. ECH can also be effective at the second harmonic.

The ECH microwave beam can be transmitted through air, which allows the source to be far from the plasma, simplifying maintenance. The ITER design includes the development of a 1 MW gyrotron operating at 170 GHz with a pulse duration of more than 500 s.

Vacuum windows will be placed outside of the neutron shielding. Alloys retaining high electrical conductivity after neutron bombardment will be used for components requiring good electrical conductivity, such as waveguides. Waveguides will have several bends to reduce neutron streaming.

The "ordinary mode" (O mode) wave has a cutoff (k → 0) where $\omega = \omega_{pe}$, so the wave will be reflected where the plasma density is high enough for this match to occur, as illustrated in Fig. 5.32.

In this example case the O mode cannot penetrate into the high density plasma near the axis, and the density gradient tends to diffract the wave away from the high density region. The extraordinary mode (X-mode) has different propagation, as shown in Fig. 5.33.

Figure 5.34 shows a more complex phenomenon. The O-mode (red curve) propagates to a cutoff, where it is converted into an X-mode (green curve), which then converts into a Bernstein wave, which is finally absorbed at the cyclotron resonance.
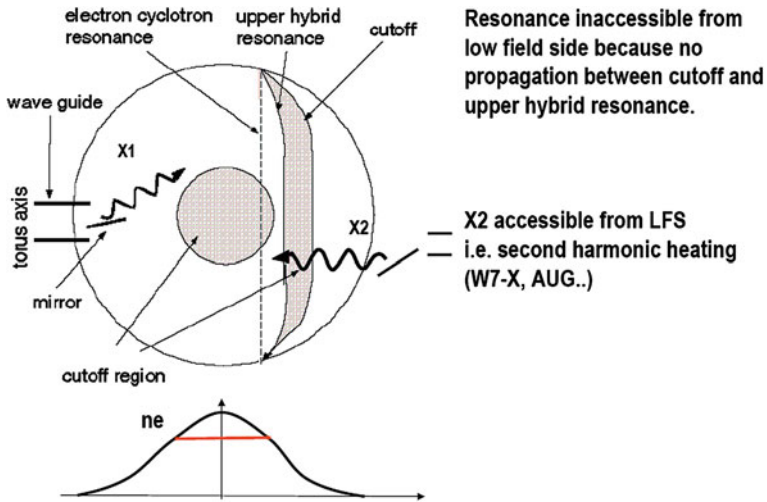
Fig. 5.33 Propagation of the X-mode from the high field side (*left side*) and from the low field side. The cutoff prevents propagation from the low field side to the resonance. The resonance can be reached from the high field side or by use of the second harmonic (Laqua 2008)
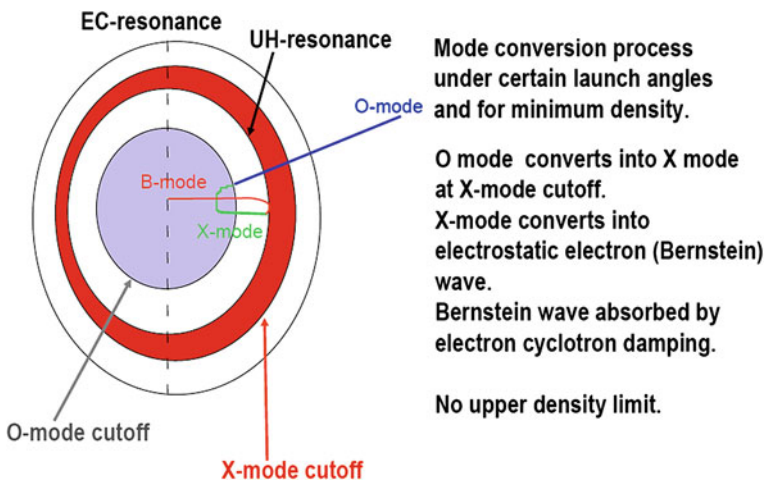
Fig. 5.34 Mode conversion of O-mode to X-mode to Bernstein wave, followed by absorption at the cyclotron resonance (Laqua 2008)

5.9.2 Heating and NTM Suppression

Figure 5.35 shows how choice of the resonance layer affects the electron temperature profile Te(r) in a stellarator.
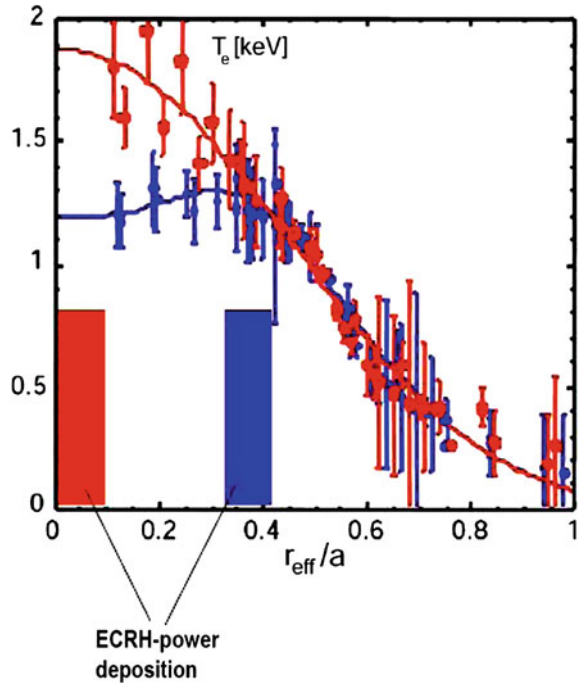
Neoclassical tearing modes (NTMs) involve the growth of "magnetic islands",
which deteriorate confinement. Application of ECCD and heating at the island
location can help alleviate this instability. This is illustrated in Fig. 5.36.
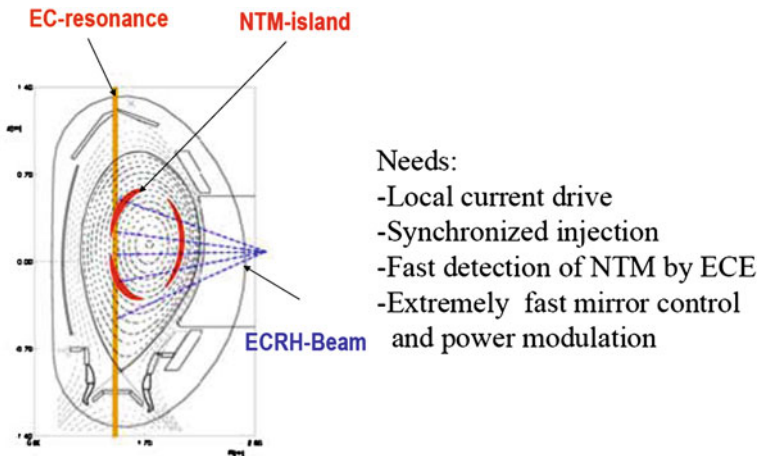
Fig. 5.36 Application of ECRH near the neoclassical tearing mode (*NTM*) island radius to
suppress the instability. Here *ECE* means an electron cyclotron emission diagnostic, which
measures the $T_e(r)$ (Laqua 2008)

ECCD has been used to suppress the NTM instability in JT-60U, and it is more effective when the microwaves are modulated (Isayama et al. 2009).

5.9.3 Wave Generation

Figures 5.37 and 5.38 show a 1 MW gyrotron developed for ECRH in the W7-X stellarator at Greifswald, Germany.

Similar gyrotrons at a higher frequency (170 GHz) are under development for ITER.

Fig. 5.37 A 1 MW 140 GHz gyrotron for the W7-X stellarator. An electron gun at the *bottom shoots* an annular (cylindrical) electron beam *upwards* through the resonator, where the magnetic field causes it to oscillate, giving up some kinetic energy to the wave before being stopped at the collector. The microwave beam is reflected by mirrors and then exits through the diamond window (Laqua 2008)
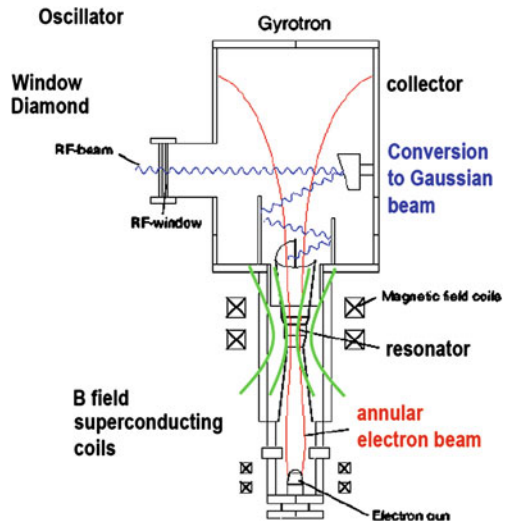
Fig. 5.38 Photograph of the W7-X gyrotron (Laqua 2008)
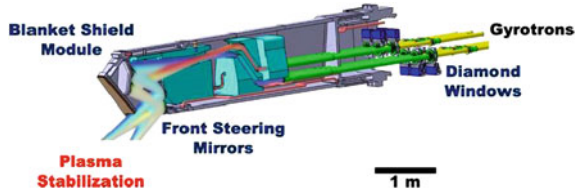
Fig. 5.39 ECH launchers for ITER (Strauss 2010)
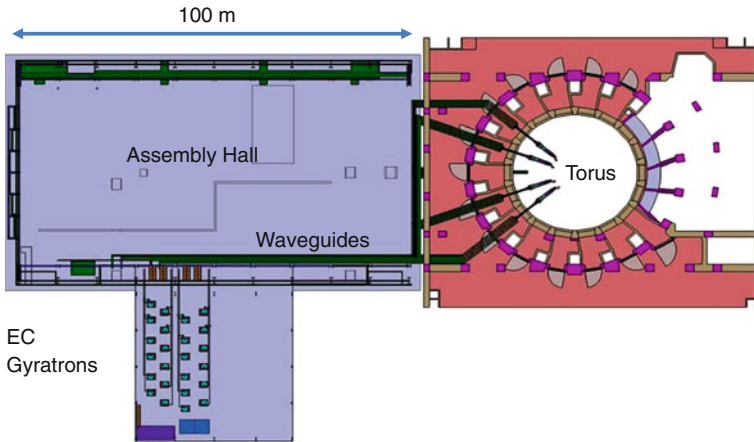
Fig. 5.40 Conceptual layout of the ITER tokamak hall, assembly hall, and ECH power supply building. Courtesy of ITER Organization

5.9.4 Transmission and Launching

ECH launchers with steerable mirrors are shown in Fig. 5.39.

Diamond windows are used because of their low power absorption and high thermal conductivity. The zigzag path reduces neutron streaming.

Figure 5.40 shows the ITER EC building next to the assembly hall and tokamak.

A series of international workshops have been conducted on ECH (Prater 2011).

5.10 Lower Hybrid Waves

The JET lower hybrid current drive (LHCD) system is shown in Fig. 5.41.

The klystrons generate the waves, and the circulators permit them to pass in the forward direction only, preventing reflected waves from damaging the klystrons.
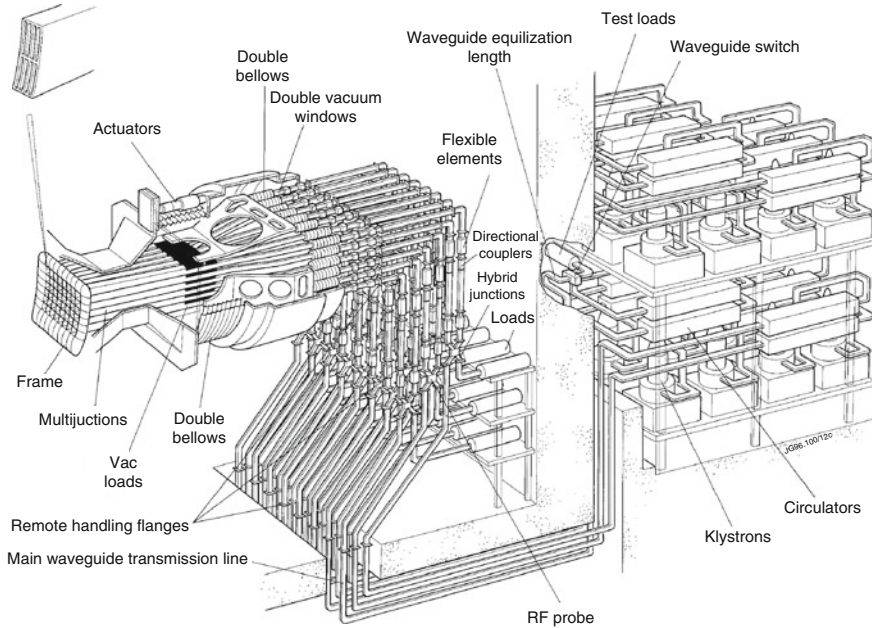
Fig. 5.41 Major components of the JET LHCD system (Jacquinot et al. 2008, Fig. 19)

Waveguides transmit the waves through couplers that adjust the wave parameters for maximum efficiency of coupling to the desired plasma modes. Windows isolate the klystrons from the plasma. Actuators adjust the position of the waveguide frame, which is mounted on double bellows for flexibility. The vacuum loads facilitate testing the system when no plasma is present.

The waveguide grill launches the waves to travel along the magnetic field as shown in Fig. 5.42.

The lower hybrid waveguide grill used in the ASDEX tokamak is shown in Fig. 5.43.

Some problems associated with electromagnetic wave heating are:

- Radiofrequency voltages can be as high as 30 kV, need to avoid breakdown.
- Plasma contact with antennas can lead to arcing.
- In case of a breakdown rapid shutoff of generators is required.
- Radiation damage to antennas can be severe.
- Vacuum windows should withstand high power fluxes without cracking.
- Waveguide bends are needed to reduce neutron streaming.

Electromagnetic wave heating offers some advantages in comparison with neutral beam heating:

- The problems of unwanted neutral gas inflow and the requirement for huge cryopumps are eliminated.
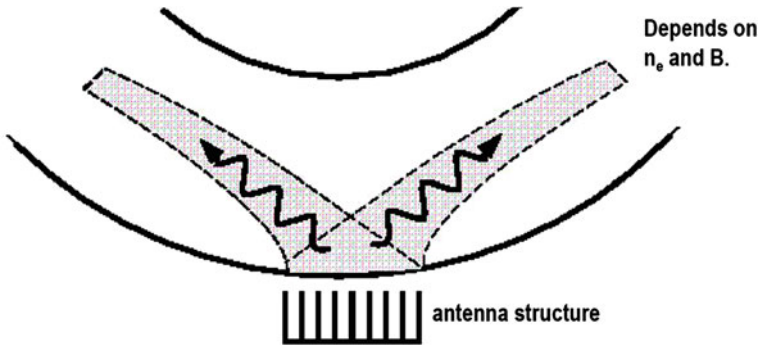
Fig. 5.42 Lower hybrid waves launched along the magnetic field (Laqua 2008)

Fig. 5.43 The ASDEX
lower hybrid waveguide grill
(Laqua 2008)

- The large neutral beam lines are replaced by smaller rf coaxial lines or wave-
  guides, permitting easier access to the torus for maintenance.
- Capital costs of rf heating are lower.

Table 5.5 Approximate efficiencies of some wave generating systems for large tokamaks and stellarators (B $\sim$ 3–6 T, n $\sim$ 10^{20} m^{-3})

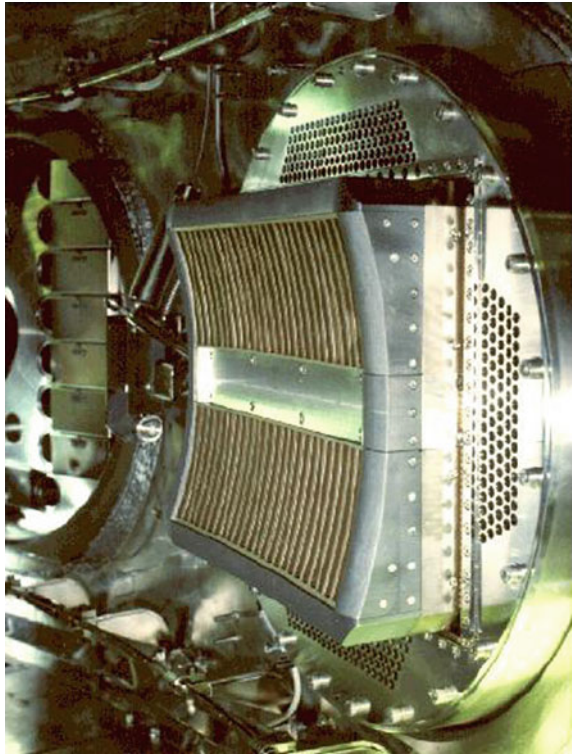| System	Electrical efficiency (%)	Remarks
1 MeV NBI	30	Reliability and cost issues
ICRF	70	Relatively inexpensive, reliable
ECRH	40	Effective, but expensive
Lower hybrid	70	Relatively inexpensive

By "efficiencies" of wave generating systems we mean (wave power generated) / (input electrical power). Table 5.5 compares the efficiencies of some wave generating systems for plasma heating.

Portions of the generated wave power are lost in transmission, penetration, coupling, and absorption (Fig. 5.23), so the actual heating power is less than the generated power, and the net heating efficiency is lower than the generation efficiency.

5.11 Current Drive and Profile Control

5.11.1 Steady State Operation

Steady state operation of a fusion reactor is very desirable, in order to avoid:

- Downtime that reduces plant availability and profits
- Fluctuations in electrical power available to the grid that must be compensated by other sources or by energy storage systems
- Temperature changes of coolant and structure that cause thermal stresses and fatigue
- Pulsing the ohmic heating coils, causing structural fatigue
- Eddy current losses that require additional refrigeration
- The need to restart the plasma and ramp up its current periodically, with possible influx of impurities or plasma disruptions.

Some methods of plasma current drive in toroidal systems are

- Magnetic Induction.
- Neutral beam injection.
- Lower hybrid resonance.
- Electron cyclotron resonance.
- Ion cyclotron resonance.
- Alpha particle "channeling".
- Helicity injection by electrodes or by sinusoidal induction.

The current density of electrons with velocity distribution function f(v) is

$$J = e \int dv \, f(v)v \tag{5.37}$$

where e = electronic charge. If the distribution function is symmetric about v = 0, then J = 0. Thus, the problem of electron current drive is to create an **asymmetric** distribution function. If the electrons were monoenergetic, then the electron current density would be

$$J = -nev \tag{5.38}$$

where n = electron density, e = electronic charge.

5.11.2 Bootstrap Current

The name "bootstrap current" refers to an English saying about "lifting oneself up by one's bootstraps" (which would normally be impossible). This current is induced by outward diffusion of plasma in the "banana regime" (high T_e, low collision frequency). The magnitude of the toroidal bootstrap current is approximately

$$J_b = (a/R_o)^{1/2}[2.44(T_e + T_i)(dn/dr) + 0.69n(dT_e/dr) - 0.42n(dT_i/dr)]/B_\theta \; (A/m^2) \tag{5.39}$$

where B_θ = poloidal magnetic field, a = minor radius, R_o = major radius, n = plasma density (m^{-3}), and T_e and T_i are the electron and ion temperatures (J) (Wesson 2011). Fueling by pellet injection can provide a good source of fuel ions in the core plasma to maintain the density gradient dn/dr. If fueling were only by cold neutral gas at the plasma edge, then the bootstrap effect would be reduced.

For low-aspect-ratio tokamaks ($R_o/a \sim 1.5$) most of the particles are trapped, and a simpler estimate may be used:

$$J_b = -(dp/dr)/ B_\theta \tag{5.40}$$

where p = plasma pressure. For example, if n = 10^{20} m^{-3} and $T_e = T_i = 10$ keV, then the pressure 2nT = 0.3 MPa. If this decreased linearly over a meter and $B_\theta = 0.3$ T, then $J_b \approx 1$ MA/m^2.

Using a large-volume plasma close to the wall for stability, JT-60U achieved a bootstrap current fraction of 92 % at an edge safety factor $q_{95} = 5.6$, with plasma density 87 % of the "Greenwald limit" (Sakamoto et al. 2009).

ITER operating scenarios to achieve high f_b are under study.

5.11.3 Lower Hybrid Current Drive

Lower Hybrid Current Drive (LHCD) is an effective non-inductive way of driving a strong toroidal current in a tokamak. The resonance condition is
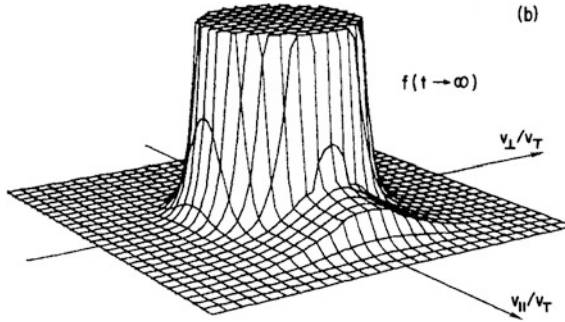
Fig. 5.44 Contours of steady-state electron velocity distribution f when lower-hybrid waves are injected with parallel-phase velocities between 3 and 5 times the thermal velocity v_T. In this picture the surface is truncated at low speeds. Reprinted with permission from Karney and Fisch (1979), © 1979 The American Institute of Physics

$$\omega - k_{ll}v_{ll} - n\omega_{ce} = 0 \tag{5.41}$$

where ω = wave frequency (rad/s), k_{ll} = wave vector component along B, v_{ll} = component of electron velocity along B, ω_{ce} = electron cyclotron frequency, and n is the mode number (not the electron density). For lower hybrid waves n = 0, and the wave travels parallel to B.

Current lasts longer when it is carried by electrons with lower collision frequencies, meaning higher energy electrons, since the collision frequency is proportional to v^{-3}, where v is the relative velocity of colliding particles.

In a tokamak magnetically trapped electrons and ions do not carry toroidal current, so energy that they absorb does not contribute to current drive.

Figure 5.44 shows the velocity distribution function of electrons heated by LHCD, with parallel phase velocities 3–5 times the thermal speed v_T. The asymmetry of the distribution function produces current drive. By convention the direction of the current is opposite to the direction of electron flow, as can be seen from the minus sign in Eq. (5.38).

One measure of the efficiency of current drive is the ratio of current driven to the input power Pd. For LHCD it is given approximately by

$$I/P \approx (v_{ph}/v_T)^2 [T_{10}/(30R_o n_{20})] \text{ A/W} \tag{5.42}$$

where $v_{ph} = \omega/k$ = wave phase velocity,

$$v_T = (kT/m_e)^{1/2} \tag{5.43}$$

is the electron thermal speed, T_{10} is the electron temperature in tens of keV, R_o is the plasma major radius (m), and n_{20} is the plasma density in units of 10^{20} m^{-3} (Fisch 1987).

For example, if ITER had $(v_{ph}/v_T)^2 \approx 20$, $T_{10} = 1$, $n_{20} = 1$, and $R_o = 6$ m, then $I/P \approx (1/9)$ A/W. If the entire 15MA current were to be provided by LHCD, the required microwave power would be 135 MW. The situation could be improved if much of the current were provided by the bootstrap effect, and if we operated at higher temperature and lower density.

For temperatures in the range $1 < T_{10} < 3$, the ratio of radiofrequency (rf) power to fusion thermal power is estimated to be approximately

$$P_{rf}/P_f \approx 15/\left[(J/P_d)(n_{20}T_{10}aR_o)^{1/2}(3T_{10} - 2)\right] \qquad (5.44)$$

where $J/P_d \approx 30$ is a current drive efficiency parameter, and a = plasma minor radius = 2 m for ITER (Fisch 1987). For a reactor with typical ITER parameters ($T_{10} = 1$, $n_{20} = 1$, a = 2 m, and $R_o = 6$ m), this yields $P_{rf}/P_f \approx 0.14$. If ITER generated 400 MW thermal power and it were converted at 40 % efficiency to electricity, the gross electrical power would be 160 MWe. The required $P_{rf} = 0.14 \times 400 = 56$ MW. If this were generated at 60 % efficiency, the required electrical power would be 93 MW, so the recirculating power fraction would be 93/160 = 58 %. Such a high recirculating power fraction would be unacceptable for an economical power plant. It is not proposed to build a power plant with ITER parameters, but this illustrates the problem of the recirculating power required for current drive, even at high efficiency (60 % assumed here).

Not all the rf power leaving the antenna or waveguide is absorbed usefully by the plasma.

- The incident waves may be scattered by edge plasma turbulence
- They may be reflected by a plasma cutoff
- Their direction may be bent by the plasma ("ray tracing" computer codes calculate the paths of the incident waves)
- They may be transformed into other types of waves ("mode conversion"). Mode conversion can be helpful by aiding penetration into the plasma or harmful by preventing the desired absorption mechanism
- They may be absorbed by a less desirable resonance.

Thus, the wave power finally absorbed for current drive will be less than the power provided by the generator.

When a tokamak plasma is started inductively and then LHCD is applied, the LHCD reduces the measured loop voltage. In some cases the plasma current may be wholly sustained by the LHCD, and the inductive current drive may be turned off (the ohmic heating coil current may be turned off or kept constant).

The "electron runaway velocity" v_R is the velocity above which the electric field force is greater than the retarding force of collisions, and the electrons continuously accelerate to higher velocities. Its magnitude is approximately

$$v_R \approx [m\Gamma/eE]^{1/2} \qquad (5.45)$$

where e = electron charge, E = electric field, and

$$\Gamma = ne^4 \ln\Lambda/4\pi\varepsilon_o^2 m^2 \qquad (5.46)$$

represents a retarding force due to collisions, n = electron density, $\ln\Lambda$ = "Coulomb logarithm" ($\ln\Lambda \sim 18$, also called L elsewhere), and ε_o = permittivity of free space. When the electric field is strong or the collision rate is weak, then v_R is low and runaway occurs easily.

Electrons with $v/v_T < 1$ are in the bulk plasma and have high collision frequencies. Electrons with $v/v_T \gg 1$ have very low collision frequencies. If we induce a current in the bulk plasma, it is quickly dissipated by collisions, but if we induce current in high energy electrons, the current tends to persist longer, so it is advantageous for current drive to push the fast electrons. This can be done by adjusting the LHCD wave phase velocity:

$$v_{ph}/\ v_T \sim 3 \text{ to } 5$$

The efficiency of generating lower hybrid waves can be $\sim 70\ \%$, and they can be efficiently transmitted by waveguides to a grill in the torus wall where they are launched with specified phase. The fraction of the wall surface required for the waveguides can be reasonably small, and the waveguides can have bends to minimize neutron streaming. A window is needed between the wave generator and the transmission waveguide, which can carry power fluxes ~ 20 MW/m^2. In order for the waves to penetrate adequately to the plasma center their parallel phase velocity should satisfy

$$\omega/k_{ll}c < 1/[1 + 15\beta/T_{10}] \qquad (5.47)$$

where $\beta = 2\mu_o p/B^2$, and p = plasma pressure. If T = 10 keV and $\beta = 0.04$, then $\omega/k_{ll}c < 0.62$. For DT reactors with $T_{10} \sim 1$ to 2 the wave parallel phase velocity should be

$$\omega/k_{ll} \sim 4.5\ v_T$$

which corresponds to resonant electrons with energies ~ 100 keV (Fisch 1987). The current drive efficiency is then

$$I/P \approx (0.6/n_{20}R_o)\,[1 + (T_{10} - 1)/3]\ \text{A/W} \qquad (5.48)$$

For example, if $T_{10} = 1$, $n_{20} = 1$, and $R_o = 6$ m, then I/P = 0.1 A/W.

LHCD has sustained the plasma current in the TRIAM-1 M superconducting tokamak for 2 h, and driven up to 3 MA in the JT-60 tokamak (Fisch 2000).

LH waves are very good at generating off-axis current drive, which is beneficial for tailoring the current density profile J(r) and the safety factor profile q(r).

LHCD in Alcator C-Mod has demonstrated current drive efficiency I/P $\approx$ 0.25/ $n_{20}R$ (A/W), consistent with expectations. During LHCD the core current (r/a < 0.44) drops and the edge current (r/a > 0.44) increases (Wilson et al. 2009).
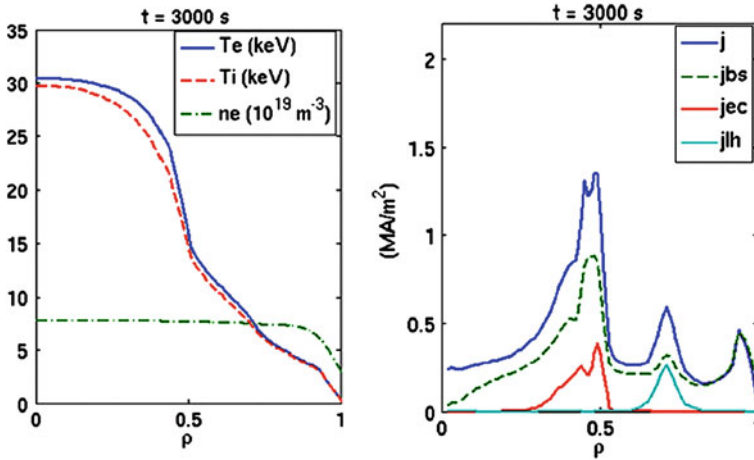
Fig. 5.45 Radial profiles of plasma temperatures and density and of current density components *jbs* (bootstrap current), *jec* (ECCD), *jlh* (LHCD) and *j* (total) in ITER for the conditions cited above (Hoang et al. 2009)

LHCD was applied to JET at 3.7 GHz with power typically modulated between 0.5 and 3 MW at 41.67 Hz. As the plasma density is increased the LHCD waves were absorbed at larger radii until a significant portion of the power was lost outside the plasma (Kirov et al. 2010).

A 20 MW, 5 GHz LHCD system for ITER is under design, but funding for its implementation is not yet allocated. The computer simulations predict fully RF steady-state $Q \sim 7$ plasmas lasting 3,000 s (non-inductive fraction ~ 97 %, resistive loop voltage ~ 2 mV) using 21 MW of ECCD power, 20 MW of ICRF power and 12 MW of LH power, as illustrated in Fig. 5.45. LHCD can provide the required off-axis current at $r/a \sim 0.7$, while ECCD helps to sustain an internal transport barrier position at $r/a \sim 0.5$ (Hoang et al. 2009).

Computer simulations indicate that loss of LH wave power to alpha particles would be negligible (Schneider et al. 2009).

Very high levels of LHCD can trigger plasma instabilities, such as the "fish-bone mode" (Cesario et al. 2009). LHCD produces hot electrons at large radii, which can limit penetration of injected fuel pellets (Budny 2010).

Some current drive can also be accomplished by ECRH, ICRH, and NBI. A combination of several techniques can be used to achieve some control over the current density profile, which could help to sustain an "internal transport barrier" (Wesson 2011).

5.11.4 Electron Cyclotron Current Drive

LHCD drives parallel fluxes and Electron Cyclotron Current Drive (ECCD) drives perpendicular fluxes. Electron cyclotron heating increases $v_\perp$, leaving v_{ll} relatively unchanged, and it can be done for electrons with high v_{ll}. As the microwaves enter the torus from the low-field side (large R) they pass through an increasing B and ω_{ce}. The electrons are resonant with the wave at the radius where

$$k_{\text{ll}} v_{\text{ll}} = \omega - \omega_{ce}(R) \qquad (5.49)$$

If the microwaves are injected from the high-field side (small R), they pass through a decreasing B and ω_{ce}.

If the microwaves are tuned to heat electrons with positive v_{ll}, their increased perpendicular energies decreases their collision frequencies, which means that they slow down more gradually than electrons with the same magnitude of v_{ll} but negative sign, which are not so heated. This makes the electron distribution function anisotropic in the parallel direction, creating an effective plasma current.

ECCD in JET at 170 GHz (2nd harmonic) has achieved efficiencies of 3–6 kA/MW at $n \approx 5 \times 10^{19}$ m^{-3} and confirmed that the current drive efficiency is inversely proportional to plasma density (Farina and Figini 2010).

5.11.5 Neutral Beam Current Drive

A neutral beam injected into a tokamak becomes ionized and trapped. The trapped ions moving in the toroidal direction provide a toroidal current density. However, electrons pulled along by the ions may neutralize this current. Then the whole plasma would rotate, but with very little current density.

One way to maintain the ion current density would be to retard the electron flow, or to use two different ion charge states. For example if a beam He^{++} (charge state $Z_b = 2$) ions were injected into a D$^+$ plasma ($Z_i = 1$), the pull on the electrons is proportional to Z^2, while the current is proportional to Z, so electrons would be pulled more strongly by the He^{++} ions, and a net current could be generated (Fisch 1987). Some of the background electrons are trapped in "banana orbits" and cannot go all the way around in the toroidal direction to neutralize the ion flow.

An approximate estimate of neutral beam current drive efficiency is

$$I/P \approx (0.6 T_{10}/n_{20} R_o)[(1/Z_b) - (1/Z_i)] \text{ A/W} \qquad (5.50)$$

where Z_b is the charge state of the ionized beam and Z_i is the charge state of the background plasma ions (Fisch 1987). This equation would imply no current drive if $Z_b = Z_i$. For the ITER example, If $T_{10} = 1$, $n_{20} = 1$, $R_o = 6$, $Z_b = 2$, and $Z_i = 1$, then I/P ≈ -0.05 A/W. (The negative sign indicates net current flow opposite to the beam direction.) If we wanted to drive 15 MA entirely by neutral beams, then the

required beam power would be 15/0.05 = 300 MW. If the efficiency of the neutral beam generator were 50 %, then the required electrical power to drive the current would be 600 MW, an impractical amount. The situation could be somewhat ameliorated by using higher temperature, lower density, and higher Z_b.

NBI can be aimed radially inwards, toroidally parallel to current density (co-injection), toroidally opposite to the current density direction (counter injection), or at any toroidal direction in between. The poloidal angle can also be controlled during design. The beam energy can be chosen to match the desired penetration depth. The angles and energy afford some control over heat deposition profile, current drive profile, poloidal rotation, toroidal rotation, and particle flow. These functions cannot be controlled independently, however, so it is necessary to focus on one or two that are most important, without causing harmful effects, such as instabilities. For example, if current drive were most important, then co-injection would be chosen at optimum depth and angles.

Figures 5.46 and 5.47 show a case where off-axis NBI was used in JT-60U to establish an internal transport barrier. This case has B = 4.4 T, I = 2.6 MA, NBI power = 15 MW, $n_o T_{io} \tau_E = 8.6 \times 10^{20}$ m^{-3} keV s, which corresponds to $Q_{DT} = 1.25$, but the configuration disrupted, due to low-n, ideal kink-ballooning modes.

When the ITB is established the ion temperature rises in about 0.6 ms, and the negative toroidal rotation velocity also increases.

NBI often causes toroidal plasma rotation. A "critical energy" W_{crit} is defined to be the energy at which beam energy losses to electrons and ions are equal. If the beam energy in the rotating frame $W \gg W_{crit}$, then plasma rotation will have little effect on the driven current. If $W \sim W_{crit}$, however, plasma rotation can reduce the current drive significantly, especially if the rotation velocity $v_\phi \geq 0.05 (2W_{crit}/M)^{1/2}$, where M = beam ion mass (Cottrell and Kemp 2009).

The neutral beam injector height and direction have a strong effect on the resulting profiles of current density and safety factor q in ITER simulations (Budny 2010).

Some problems of neutral beam current drive are

- High power required.
- High voltage breakdown.
- Lifetime of electrodes.
- Neutral gas in injection ports.
- Very high vacuum pumping speeds, large cryopanels and refrigeration systems required.
- Limited tunabililty of beam parameters (energy, current, direction).
- Neutron streaming out beam ports and activating the whole beamline. (Bends to attenuate neutrons are not feasible).
- Reliability and maintenance of radioactive NBI systems.
- Cost.

In view of these issues it would be good if DEMO could work without requiring NBI.

Fig. 5.46 Profiles of density, temperatures, and safety factor in JT-60U with an ITB established by off-axis NBI (Ishida and JT-60 Team 1999)
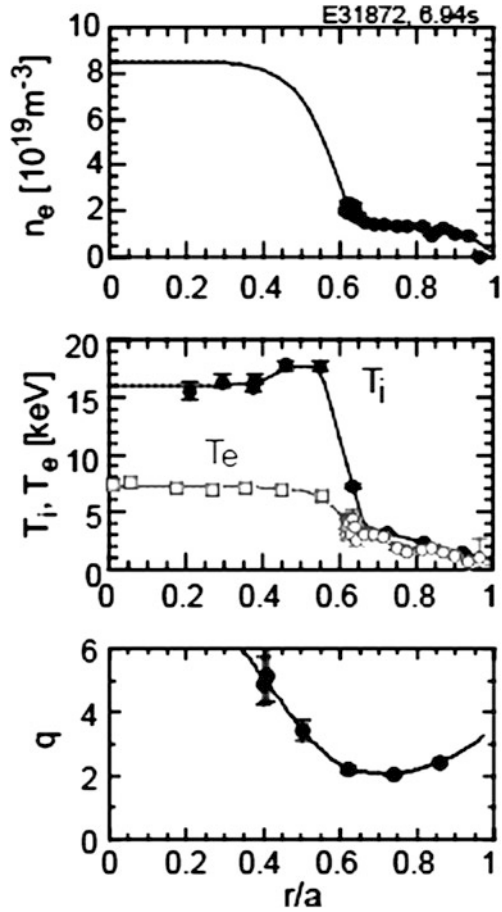
5.11.6 ICRF Current Drive

Some current might be driven by ICRF heating, but it is less promising for ITER than current drive by LHCD, ECCD, and NBI (Budny 2010). Current drive by ICRF waves is discussed in Chap. 6 of Kikuchi et al. (2012).

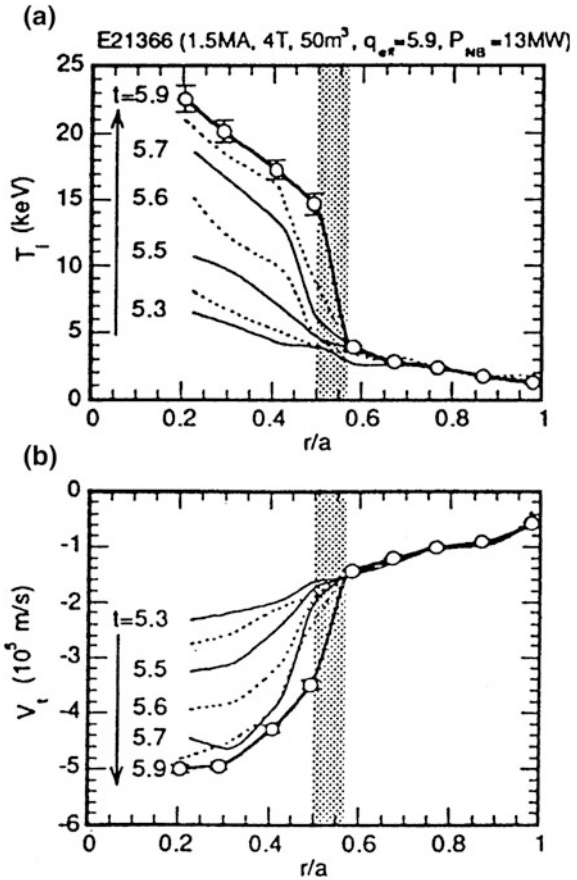### 5.11.7 Alpha Particle Channeling

The goal is for the 3.5 MeV alpha particles to transfer their energy to drive plasma current. The alpha particle gyrofrequency is

$$\Omega = 2eB/M \ (rad/s) \tag{5.51}$$

Fig. 5.47 Variation of ion temperature profile and rotation velocity profile during establishment of the ITB of the previous figure (Koide et al. 1995)

where M = alpha particle mass. For example, if B = 5 T, then $\Omega = 2.4 \times 10^5$ rad/s. The interactions are described in terms of three parameters that tend to remain constant in the absence of collisions or interactions with waves:

$$\mu = mv_\perp^2/2B = \text{"magnetic moment"} \tag{5.52}$$

$$\varepsilon = \mu B + mv_\parallel^2/2 = \text{kinetic energy} \tag{5.53}$$

$$P_\phi = R(mB_\phi v_\parallel/B - eA_\phi) = \text{canonical angular momentum} \tag{5.54}$$

For current drive to occur the invariance of the magnetic moment can be broken by interaction with an ion Bernstein wave (IBW) that is externally generated. The $k_\parallel$ of the launched IBW changes sign at the "mode conversion layer", which

facilitates extraction of energy from the alpha particles. Then the alpha particle can diffuse perpendicular to B by interaction with a second wave, such as a toroidal Alfven eigenmode (TAE) wave, while losing energy to that wave.

The induced waves and collisionless slowing down of alpha particles (called "alpha channeling") could induce an electronic current in the plasma. Experimental data from the TFTR experiment indicate that the perpendicular diffusion rate was much faster than predicted by simple quasi-linear theory (Fisch 2000).

5.11.8 Helicity Injection

By definition the helicity K in a volume bounded by a magnetic surface is

$$K = \int dV \mathbf{A} \cdot \mathbf{B} \tag{5.55}$$

where B is the magnetic field, A is the magnetic vector potential satisfying $\mathbf{B} = \nabla \times \mathbf{A}$, and dV is a volume element. Plasmas tend to conserve helicity while relaxing to a minimum energy state. Helicity injection induces current flow in the plasma. The rate of change of helicity is described by

$$\partial K/\partial t + \nabla \cdot \mathbf{Q} = -2\eta \mathbf{J} \cdot \mathbf{B} \tag{5.56}$$

where the helicity flux is

$$\mathbf{Q} = \mathbf{B}\Phi_{el} + \mathbf{E} \times \mathbf{A} \tag{5.57}$$

Φ_{el} = electric potential, $\mathbf{E}$ = electric field, $\mathbf{J}$ = inductive current density, and η = plasma resistivity. Helicity can be injected by passing an electric current along a magnetic flux surface, and it is dissipated (lost) by ohmic heating. If we apply a voltage V around a toroidal loop the helicity injection rate is

$$\partial K/\partial t = 2V\Phi_T \tag{5.58}$$

where Φ_T is the toroidal magnetic flux. A similar equation applies to a poloidal loop and poloidal flux. Bellan (2006) discusses the mathematical and topological aspects of magnetic helicity.

Helicity has been injected into small toroidal devices by applying a voltage to electrodes in the poloidal direction, resulting in poloidal current flow that evolved into toroidal current flow as the plasma adjusted towards a minimum energy state.

Coaxial helicity injection (CHI) has been used in the National Spherical Torus Experiment (NSTX). The method is shown in Fig. 5.48.

The divertor coils generate a magnetic flux Φ_T (blue circle). The capacitor bank voltage V drives current along this field in the counterclockwise direction (big orange arrow). This voltage and flux produce the $\partial K/\partial t = 2\ V\Phi_T$ term that injects helicity. The $J_{pol} \times B_{tor}$ force pushes plasma upwards, and magnetic reconnection results in a toroidal plasma current.
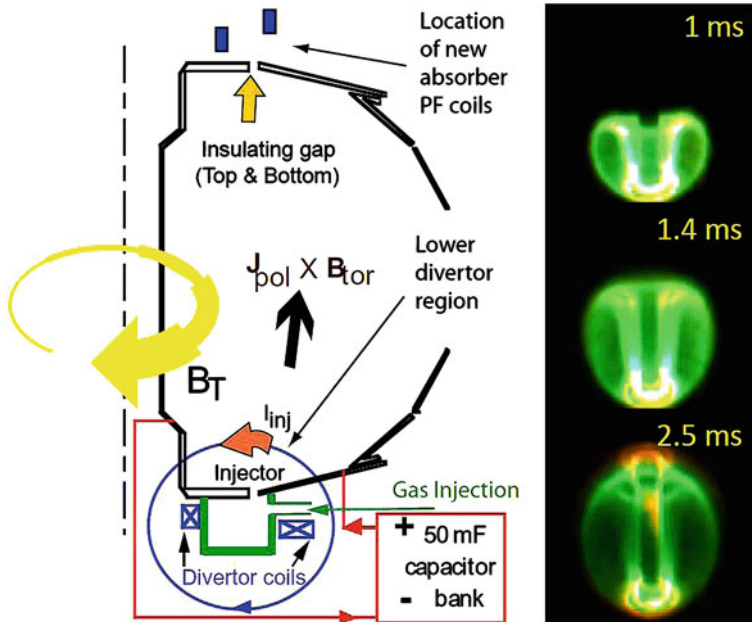
Fig. 5.48 a On the *left*, is a *line drawing* showing the main components in NSTX required for plasma startup using the CHI method. *Top-right* **b** fast camera fish-eye image of the plasma during the early phase of plasma growth at the *bottom* and **c** later in time after the CHI started discharge has filled the vessel. The *vertical black post* in the center contains both poloidal and toroidal field coils (Raman et al. 2009)

There are five requirements for success of this CHI method:

- Capacitor bank energy must be sufficient to generate a current that can "break the bubble" and inject plasma upwards.
- The voltage must be high enough that the plasma fills the chamber quickly.
- The capacitor bank energy must be sufficient to fully ionize and heat all the injected gas.
- The maximum plasma current I that can be generated is limited by $\frac{1}{2}LI^2 < \frac{1}{2}CV^2$ where L = plasma inductance, C = capacitance, V = capacitor voltage.
- The "footprints" of the divertor flux on the electrodes must be sufficiently narrow (controlled by coil and electrode design).

An injector current of below 10 kA has induced a plasma current up to 300 kA, with an amplification factor over 50. In some experiments CHI drove toroidal currents ~ 300 kA, which were then ramped up to higher currents using the ohmic heating transformer. For success of the ramp-up the radiated power must be kept below the input power, or else an additional heating method is needed. Additional heating by ECRH can ionize low-Z impurities, reducing plasma resistivity and
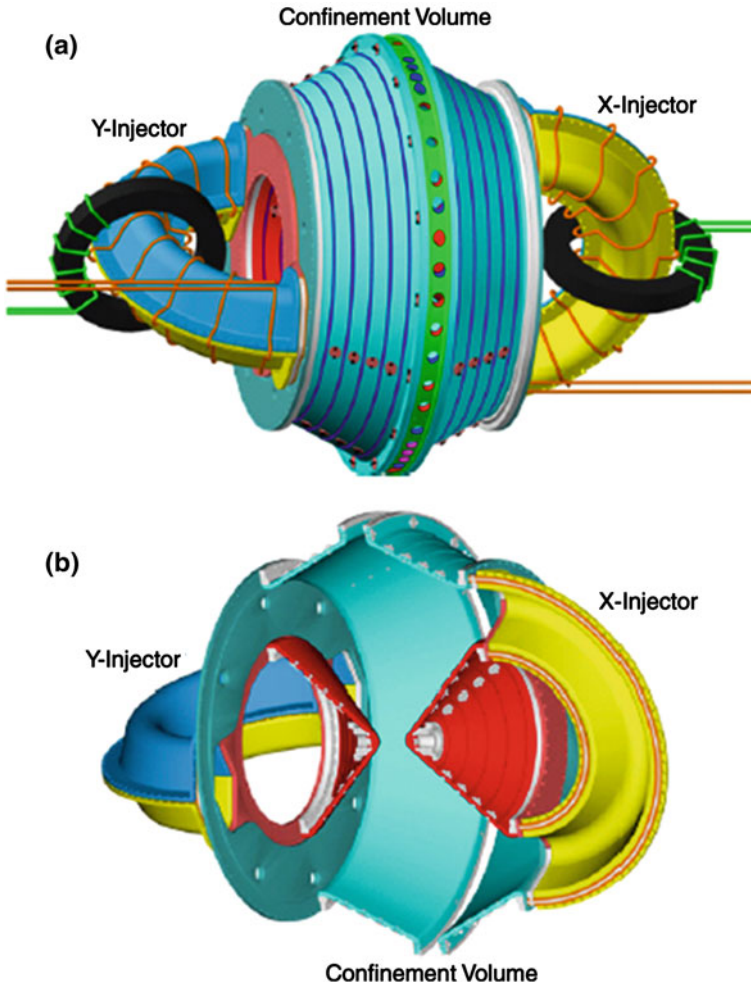
Fig. 5.49 The HIT-SI device consists of two semi-toroidal injectors attached to a central confinement volume. **a** Injector loop voltage coils are shown in *green* with the injector flux coils shown in *orange*. Solid transformer coils are only depicted for loop voltage circuit clarity, as in reality air-core transformers are used. Thin *lavender* rings identify several of the axial flux loops used to measure the total toroidal current. **b** A cutaway of the HIT-SI vacuum vessel from the X-injector to the Y-injector annulus, making evident the bow-tie cross section of the confinement volume (viewing angle slightly rotated) (Ennis 2010)

increasing plasma current. The NSTX-Upgrade experiment should achieve non-inductively driven currents over 0.5 MA (Raman et al. 2009, 2011).

The Helicity Injected Torus-Steady Inductive (HIT-SI) experiment, Fig. 5.49, consists of a toroidal confinement volume with two external loops, the X-injector and the Y-injector. Each injector has toroidal field coils producing flux Φ_T and a ring-shaped inductor that generates a sinusoidal voltage V. The voltage along the

toroidal flux causes sinusoidal helicity injection $\partial K/\partial t = 2\ V\Phi_T$. The X and Y injectors are 90° out of phase, so that the total helicity injection rate is proportional to $\sin^2\theta + \cos^2\theta = 1$, hence constant.

The width and outer radius of the flux-conserver chamber are each <0.6 m, and the minor radii of the injectors are ~ 0.1 m. Using injector voltages ~ 300–450 V modulated at 5.8 kHz with 6 MW power input they achieved formation of a spheromak plasma with toroidal plasma current >30 kA and poloidal flux 6 times larger than the injector flux. When the spheromak flux was lost into the metallic walls, the current direction flipped (Ennis et al. 2010). This experiment is very small, so plasma-wall interactions and impurities make it difficult to sustain the plasma. A much larger experiment is needed to adequately test this concept (Jarboe et al. 2012) (See also Sect. 1.3.4).

5.12 Summary

Compression is not used in tokamaks and stellarators, but is a key feature of magnetized target fusion.

Ohmic heating is inherent in tokamaks, which must have a strong toroidal current, but not in stellarators, which do not require a plasma current for equilibrium. Ohmic heating is usually insufficient to ignite a tokamak, so auxiliary heating methods are needed.

If non-inductive current drive can be successful, then the central solenoid should be avoided. The absence of a central solenoid would facilitate lower aspect ratio, higher beta, and higher power density at a given magnetic field. The ability to start up a tokamak non-inductively is under study in several experiments, such as NSTX, which has achieved 300 kA toroidal current.

Neutral beam injection current drive is valuable for heating and for profile control at modest density. The injector is complex and expensive, requiring very high vacuum pumping speed, and the large port permits neutron streaming, creating shielding problems. High voltage injectors (1 MeV) using negative ion beams are under development for ITER.

ICRH is relatively inexpensive, with well-developed components. It provides efficient heating, but not strong current drive. Plasma-antenna interactions can lead to plasma impurities.

ECRH is very effective and helps control profiles of electron temperature and current density. Long-pulse, high-power generators (1 MW) are under development for ITER.

LHCD is effective and can help with profile control. It works best at low density.

Coaxial helicity injection in NSTX has achieved toroidal currents over 50 times the injector current. The HIT-SI device uses sinusoidally-pulsed magnet coils to induce the required voltage and flux in external loops, without using electrodes, which could release impurities, but it needs to be tested in a larger experiment.

Table 5.6 Summary of heating/current drive methods. Based partly on (Laqua 2008)

Method	Heating	Current drive	Disadvantages
Alpha heating	Excellent	Maybe by channeling	Need to exhaust He ash
Ohmic	Simple, good for startup	Effective at T < 1 keV	Pulsed only, ineffective at high T, uses central solenoid coil
Compression	Effective heating	Not used for current drive	Uses too much plasma volume, pulsed, fatigue problems
NBI	Effective, controls rotation, can be somewhat localized for profile control	Effective at low n	Ineffective at high n, complex, requires 1 MeV negative ion beams, reliability problems, expensive
ICRH	Effective, central heating, inexpensive	Low effectiveness	Plasma-antenna interactions can damage antenna and yield impurities
ECRH	Effective, can be localized for profile control	Effective, can help control current density profile	Expensive, heats only electrons
LH	Effective, can be localized for profile control	Good at low n, most effective	Waveguide close to plasma can cause impurity injection, not good at high n
Helicity injection	Gives rise to some Ohmic heating	Useful for startup and sustainment	Plasma contact with electrodes injects impurities (avoided in HIT-SI experiment which uses sinusoidal inductive helicity injection)

Plasma heating methods are summarized in Table 5.6.

With any tokamak current drive system it will be important to attain a high **bootstrap current** fraction. We should use methods that couple effectively to the plasma, attain high efficiency of generation and transmission, and are affordable; supplemented by modest amounts of less efficient and more expensive systems as needed for profile control. If high input power is required for current drive, then the attainable Q value of the ignited tokamak could be uneconomically low.

5.13 Problems

5.1. Estimate the ohmic heating power per unit volume in a tokamak plasma where $J_\parallel = 10^6$ A/m^2, n = 5×10^{19} m^{-3}, and B = 4 T, (a) if $T_e = 0.2$ keV, (b) if $T_e = 2$ keV.

5.2. A cylindrical low-beta plasma is compressed radially by tripling B. Initially $T_\parallel = T_\perp = 1$ keV. What are the final temperatures (a) if the plasma is collisionless, (b) if collisions are dominant?

5.3. A collisional, cylindrical, high-beta plasma is compressed radially by tripling B. By what factor does the temperature increase?

5.4. A collisional, low-beta, toroidal plasma is compressed by decreasing the major radius to 80 % of its original value, with B_o constant. By what factor does the temperature increase?

5.5. Assume that a plasma gun uses electrical energy from a 20 kJ capacitor bank to inject a plasma blob of 10^{18} ions with $T_i = 0.8$ keV, $T_e = 0.1$ keV. What is the efficiency = (plasma energy output)/(electrical energy input) of this heating device?

5.6. Estimate the required deuterium atom beam energy for effective penetration into a DT plasma with $n = 2 \times 10^{20}$ m^{-3}, $T_e = 10$ keV, and a = 2 m. What are the neutralization efficiencies of D^+ and D^- beams at this energy?

5.7. Consider a laboratory plasma experiment with $B_{max} = 0.5$ T, $n = 3 \times 10^{18}$ m^{-3}. If you have generators at 1 MHz, 100 MHz, and 10 GHz available, what means might be used to couple the energy to the plasma?

5.8. Assume that ITER generates 400 MW steady state thermal power. Assume that $I/P = 0.1$ A/W for LHCD and 0.05 A/W for NBI. If the bootstrap current fraction is 64 %, and the remaining current is to be driven half by LH, and half by NBI, what is the maximum value of Q that could be attained, ignoring other input powers?

5.14 Review Questions

1. Why does ohmic heating fail at high temperatures?
2. What phenomena can increase plasma resistivity?
3. What causes electron runaway, and why is it undesirable?
4. Why will plasma compression not be used on large tokamaks?
5. Why is charged particle injection not used in tokamaks?
6. Can plasma guns be used to heat a tokamak plasma? If so, how does it work?
7. About how much penetration is desired for neutral beam injection to be effective?
8. Sketch a neutral beam injector and explain how it works.
9. Why are negative ion beams used for high energy neutral beam injectors?
10. What energy neutral beam injection will be used for heating in ITER?
11. What are the stages of wave heating, beginning with generation?
12. Why should a waveguide have several bends in it?
13. What is a "second harmonic resonance"?
14. How are radiofrequency waves transmitted and coupled to the plasma?
15. How are microwaves transmitted and coupled to the plasma?
16. How can sputtering from ICRF antennas be reduced?
17. How can the growth of magnetic islands be reduced?

18. Name two advantages of wave heating in comparison with neutral beam injection.
19. Under what conditions can a bootstrap current be generated? About what fraction of the total plasma current has been driven by this method in experiments?
20. What kind of fueling can help promote the bootstrap current?
21. Approximately what value to I/P (A/W) can be achieved for an ITER example case by LHCD? By NBI?
22. What phenomenon is described by the equation $\partial K/\partial t = 2\,V\Phi_T$?
23. How can helicity injection be done experimentally? What are the general requirements for capacitor bank voltage and energy?
24. What is the advantage of the HIT-SI experiment?

References

Alexeff I (1975) A theoretical predication of the observed plasma heating in the compression experiment at Ito's group at Osaka University, IEEE Trans Plasma Sci PS-3, 15–17

Badger B et al (1979) NUWMAK, A tokamak reactor design study. University of Wisconsin Report UWFDM-330

Bellan PM (2006) Fundamentals of plasma physics. Cambridge University Press

Bobkov V et al (2010) Assessment of compatibility of ICRF antenna operation with full W wall in ASDEX Upgrade. Nucl Fusion 50:035004, (11 pp)

Bostick WH, Prior W, Grunberger L, Emmert G (1966) Pair production of plasma vortices. Phys Fluids 9:2078

Bucalossi J (2010) Tore Supra, Towards steady-state tokamak operation, Karlsruhe International School on Fusion Technologies September 6–17

Budny RV (2010) Current control in ITER steady state plasmas with neutral beam steering. Phys Plasmas 17:042506

Cesario R et al (2009) Lower hybrid wave produced supra-thermal electrons and fishbone-like instability in FTU. Nucl Fusion 49:075034 (7 pp)

Chen FF (1984) Introduction to plasma physics and controlled fusion, vol 1. Plasma physics. Springer

Colas L et al (2006) Key results of long pulse ICRH operation in Tore Supra. Nucl Fusion 46:S500–S513

Cottrell GA, Kemp R (2009) Effect of plasma rotation on the beam-driven current. Nucl Fusion 49:042001 (5 pp)

Day I, Surrey E, Jones T, Ciric D, Stork D (2010) Introduction to neutral beam injection technology. Karlsruhe International School on Fusion Technologies, 7 Sept 2010

De Lazzari D, Westerhof E (2010) On the merits of heating and current drive for tearing mode stabilization. Nucl Fusion 49:075002 (8 pp), and Erratum (2010) Nucl Fusion 50:079801 (2 pp)

Dolan TJ (1982) Fusion research. Pergamon Press, Elmsford, NY

Ennis DA et al (2010) New understandings and achievements from independent-injector drive experiments on HIT-SI. Nucl Fusion 50:072001 (4 pp)

Farina D, Figini L (2010) Investigation of electron cyclotron wave absorption and current drive in JET. Nucl Fusion 50:095007

Fisch NJ (1987) Theory of current drive in plasmas. Rev Mod Phys 58:175–234

Fisch NJ (1993) Review of current drive theory: selected topics. Plasma Phys Controlled Fusion 35:A91–A104

Fisch NJ (2000) Physics of alpha channeling and related TFTR experiments. Nucl Fusion 40:1095–1100

Fukumoto N, Ogawa H, Nagata M, Uyama T, Shibata T, Kashiwa Y, Kusama Y (2004) Characteristics of modified CT injector for JFT-2 M. Fusion Eng Des 70:289–297

Goldston RJ, Rutherford PH (1995) Introduction to plasma physics. Taylor and Francis, London

Hoang GT et al (2009) A lower hybrid current drive system for ITER. Nucl Fusion 49:075001 (11 pp)

Houlberg WA, Mense AT, Attenberger SE (1980) Neutral beam energy and power requirements for expanding radius and full bore startup of tokamak reactors. Nucl Fusion 20:811–820

Isayama A et al (2009) Neoclassical tearing mode control using electron cyclotron current drive and magnetic island evolution in JT-60U. Nucl Fusion 49:055006 (9 pp)

Ishida S, JT-60 Team (1999) JT-60U high performance regimes. Nucl Fusion 39:1211 (Fig. 4)

Jacquinot J et al (2008) JET mission and highlights during 1978—1999. Fusion Sci Technol 53:887 (Figure 19. Copyright by the American Nuclear Society, LaGrange Park, Illinois, USA)

Jacquinot J et al (2009) Progress on the heating and current drive systems for ITER. In: Proceeding of the 25th symposium on fusion technology (SOFT-25). Fusion Engineering and Design, vol 84, pp 125–130

Jarboe TR, Victor BS, Nelson BA, Hansen CJ, Akcay C, Ennis DA, Hicks NK, Hossack AC, Marklin GJ, Smith RJ (2012) Imposed dynamo current drive. Nucl Fusion 52:083017 (9 pp)

Karney CFF, Fisch NJ (1979) Numerical studies of current generation by radio-frequency traveling waves, Phys Fluids 22:1817

Kikuchi M, Lackner K, Tran MQ (2012) Fusion Physics, International Atomic Energy Agency, Vienna, Austria

Kirov JK et al (2010) LH power deposition and CD efficiency studies by application of modulated power at JET. Nucl Fusion 50:075003 (17 pp) doi:10.1088/0029-5515/50/7/075003

Koide Y, Ishida S, Kikuchi M, Mori M, Tsuji S, Nishitani T, Kawano Y, Hatae T, Fujita T, Ozeki T, Shirai H, Kamada Y, Yoshino R, Ninomiya H, Azumi M, JT-60 Team (1995) Improved confinement and transport barrier in the JT-60U high β_p H mode. International atomic energy agency, plasma physics and controlled nuclear fusion research 1994. In: Proceedings of the fifteenth international conference on plasma physics and controlled nuclear fusion research held by the International Atomic Energy Agency in Seville, 26 Sept–1 Oct 1994, vol 1. IAEA, Vienna, 1995, paper IAEA-CN-60/A2-3 (Fig. 6)

Lancellotti V et al (2006) TOPICA: an accurate and efficient numerical tool for analysis and design of ICRF antennas. Nucl Fusion 46:S476–S499

Laqua H (2008) Plasma waves and RF-plasma heating. Summer School on Fusion Technology, Karlsruhe Institute of Technology, Germany

Litvak A, Sakamoto K, Thumm M (2011) Innovation on high-power long-pulse gyrotrons. Plasma Phys Controlled Fusion 53:124002 (14 pp)

Mendes A et al (2010) Reduction of RF-sheaths potentials by compensation or suppression of parallel RF currents on ICRF antennas. Nucl Fusion 50:025021 (17 pp)

Messiaen A et al (2010) Performance of the ITER ICRH system as expected from TOPICA and ANTITER II modeling. Nucl Fusion 50:025026 (21 pp)

Messiaen A, Vervier M, Dumortier P, Lamalle P, Louche F (2006) Study of the ITER ICRH system with external matching by means of a mock-up loaded by a variable water load. Nucl Fusion 46:S514–S539

Milanesio D et al (2010) ITER ICRF antenna analysis and optimization using the TOPICA code. Nucl Fusion 50:025007 (10 pp)

Perkins LJ, Ho SK, Hammer JH (1988) Deep penetration fueling of reactor grade tokamak plasmas with accelerated compact toroids. Nucl Fusion 28:1365

Phillips CK et al (2009) Spectral effects on fast wave core heating and current drive. Nucl Fusion 49:075015 (8 pp)

Portone A et al (2008) ITER TF coil ripple: Evaluation of ripple attenuation using Fe insert and of ripple enhancement produced by TBM. Fusion Eng Des 83:1619–1624

Prater R (2011) Electron cyclotron emission and electron cyclotron resonance heating (EC-16). In: Proceedings of th 16th joint workshop. World Scientific, Singapore

Raman R (2006) Advanced fueling system for use as a burn control tool in a burning plasma device. Fusion Sci Technol 50:84

Raman R (2008) Advanced fueling system for ITER. Fusion Eng Des 83:1368–1374

Raman R et al (1993) Design of the compact toroid fueler for center-fueling-Tokamak-de-Varennes. Fusion Technol 24:239–250

Raman R et al (1994) Experimental demonstration of non disruptive, central FUELING of a Tokamak by compact toroid injection. Phys Rev Lett 73:3101

Raman R, Martin F, Haddad E, St-Onge M, Abel G, Côté C, Richard N, Blanchard N, Mai HH, Quirion B, Lachambre J-L, Gauvreau J-L, Pacher GW, Décoste R, Gierszewski PJ, Hwang DQ, Hirose A, Savoie S, Leblanc B-J, Mclean H, Xiao C, Stansfield BL, Côté A, Michaud D, Chartre M (1997) Experimental demonstration of tokamak fuelling by compact toroid injection. Nucl Fusion 37:967–972

Raman R et al (2009) Solenoid-free plasma startup in NSTX using transient CHI. Nucl Fusion 49:065006 (6 pp)

Raman R, Mueller D, Jarboe TR, Nelson BA, Bel MG, Gerhardt S, LeBlanc B, Menard J, Ono M, Roquemore L, Soukhanovskii V (2011) Experimental demonstration of tokamak inductive flux saving by transient coaxial helicity injection on national spherical torus experiment. Phys Plasmas 18:092504

Sakamoto Y et al (2009) Development of reversed shear plasmas with high bootstrap current fraction towards reactor relevant regime in JT-60U. Nucl Fusion 49:095017 (8 pp)

Schneider M et al (2009) Self-consistent simulations of the interaction between fusion-born alpha particles and lower hybrid waves in ITER. Nucl Fusion 49:125005 (18 pp)

Seidl M (1979) A review of electron-beam heating of magnetic-mirror confined plasmas, with application to the tandem mirror experiment. Lawrence Livermore National Laboratory report UCRL-52759, 10 Apr 1979

Sheffield J (1994) The physics of magnetic fusion reactors. Rev Mod Phys 66:1015

Stix TH (1972) The physics of wave heating. Project Matterhorn report MATT-929

Stix TH (1992) Waves in Plasmas. American Institute of Physics, New York

Strauss ID (2010) ECRH upper port plugs and diamond window technology. In: 4th Karlsruhe international summer school on fusion technologies

Taylor JB (1974) Relaxation of toroidal plasma and generation of reverse magnetic fields. Phys Rev Lett 33:1139–1141

Taylor G et al (2010) Advances in high-harmonic fast wave physics in the national spherical torus experiment. Phys Plasmas 17:056114

Tokamak Fusion Test Reactor Final Design Report (1978) Princeton plasma. Physics Laboratory, report PPPL-1475, Aug 1978

Wagner CE (1981) Possibility of achieving ignition in a high-field ohmically heated tokamak, Phys Rev Lett 46:654–657

Wesson J (2011) Tokamaks, 4th edn. Oxford University Press, Oxford

Wilson JR et al (2009) Lower hybrid heating and current drive on the Alcator C-Mod tokamak. Nucl Fusion 49:115015 (8 pp)